UNIVERSITY OF ICELAND

M.S. Thesis

in Bioengineering

Prediction of metabolic flux differences across flow conditions in endothelial cells

John Rafael

June 2024

FACULTY OF INDUSTRIAL ENGINEERING, MECHANICAL ENGINEERING AND COMPUTER SCIENCE

Prediction of metabolic flux differences across flow conditions in endothelial cells

John Rafael

Thesis submitted in partial fulfillment of a
Magister Scientiarum degree in Bioengineering

M.S. Committee
Óttar Rólfsson
Adrian Lopez Garcia de Lomana
Sigurður Brynjólfsson

Examiner
Steinn Guðmundsson

Faculty of Industrial Engineering, Mechanical Engineering and Computer Science
School of Engineering and Natural Sciences
University of Iceland
Reykjavik, June 2024

Prediction of metabolic flux differences across flow conditions in endothelial cells

60 ECTS Thesis submitted in partial fulfillment of a *Magister Scientiarum* in Bioengineering

Faculty of Industrial Engineering, Mechanical Engineering and Computer Science
School of Engineering and Natural Sciences
University of Iceland
VR II, Hjarðarhaga 2-6 107, Reykjavik
Iceland

Telephone: 525 4000

Bibliographic information:
John Rafael, 2024, *Prediction of metabolic flux differences across flow conditions in endothelial cells*, M.S. thesis, Faculty of Industrial Engineering, Mechanical Engineering and Computer Science, University of Iceland, pp, 65.

Abstract

Endothelial cells (ECs) play a crucial role in vascular health, with their metabolic states dictating transitions between quiescent and angiogenic phases. Despite known influences of biophysical cues like shear stress from blood flow on EC biology. comprehensive insights into how flow regimes modulate EC metabolism remain elusive. Addressing this gap, our study employs genome-scale metabolic models (GEMs) generated through the application of the rFASTCORMICS approach, refined by the integration of transcriptomics and metabolomics data. This novel methodology elucidates the detailed impact of flow on EC metabolic states. Our results uncover significant alterations in the TCA cycle, branched-chain amino acids, eicosanoids, glutamine, and glutamate metabolism, providing new insights linked to the pathogenesis of vascular diseases. These findings not only advance our understanding of endothelial metabolism under varying flow conditions but also offer potential pathways for therapeutic intervention.

Útdráttur

Æðaþelsfrumur (e. Endothelial cells, EC) gegna lykilhlutverki í blóðrásarkerfinu þar sem efnaskiptaferli þeirra hafa áhrif á umbreytingu úr kyrrstæðufasa (e. quiescence) yfir í æðarmyndunarfasa. Enn skortir heildstæða sýn á það hvernig efnaskiptum æðaþelsfrumna er stjórnað af mismunandi tegundum æðarflæðis, þrátt fyrir góðan skilning á lífeðlisfræðilegum áhrifaþáttum á blóðflæði. Markmið þessarar rannsóknar er að fylla í þekkingareyður með notkun efnaskiptalíkana á erfðamengisskala (e. Genome-scale metabolic models, GEMs) sem búin eru til með hjálp rFASTCORMICS -nálgunarinnar studdrar af gögnum úr umritunar- og efnaskiptamengjum. Þessi nýja aðferðafræði afhjúpar í smáatriðum áhrif blóðflæðis á efnaskiptaástand æðaþelsfrumna. Niðurstöður okkar sýna fram á marktækar breytingar í sítrónusýruhringnum (TCA), greinóttum amínósýrum, eikosanóíðum, glútamíni og glútamati, sem varpar ljósi á myndun æðasjúkdóma. Þessar niðurstöður dýpka skilning okkar á efnaskiptaferlum æðaþelsfrumna undir mismunandi blóðflæði auk þess sem þær gefa góða vísbendingu um þau efnaskipti sem gætu skipt hvað mestu máli í meðferðum framtíðarinnar.

Table of Contents

List of Figures

List of Tables

Abbreviations

ECs: Endothelial cells

SS: Shear-stress

GCX: Glycocalyx

PGs - Proteoglycans

GAGs: Glycoaminoglycans

HA: Hyaluronan

NO: Nitric oxide

PKD1: Polycystins 1

PKD2: Polycystins 2

eNOS – Endothelial nitric oxide synthase

FA: Fatty acids

ATP: Adenosine triphosphate

OXPHOS: Oxidative phosphorylation

TCA: Tricarboxylic acid

ROS: Reactive oxygen species

EGL: Endothelial glycocalyx

UDP: Uridine diphosphate

KLF2: Krüppel-like factor 2

BCAAs: Branched-chain amino acids

AAs: Amino acids

T2DM: Type 2 diabetes

FAO: Fatty acid oxidation

5-MTP: 5-methoxytryptophan

OAA – Oxaloacetate

CoA – Coenzyme A

dNTP – deoxynucleotide triphosphate

CPT1a – Carnitine palmitoyltransferase 1a

NADPH – Nicotinamide adenine dinucleotide phosphate (reduced)

S1P – Sphingosine 1-phosphate

GPCRs – G-protein-coupled receptors

EDGs – Endothelial genes

GEMs – Genome-scale metabolic models

BiGG – Biochemical, Genetic, and Genomic

HMR2 – Human Metabolic Reaction 2

iHSA – improved reconstruction of human metabolism

GPR – Gene-protein-reaction

GIMME – Gene Inactivity Moderated by Metabolism and Expression

iMAT – Integrative Metabolic Analysis Tool

COBRA – Constraint-Based Reconstruction and Analysis

FBA – Flux Balance Analysis

FVA – Flux Variability Analysis

pFBA – parsimonious Flux Balance Analysis

H&R – Hit-and-Run

ACHR – Artificial Centering Hit-and-Run

tINIT – Task-driven model reconstruction algorithm

EGM2 – Endothelial Growth Medium 2

RNA – Ribonucleic acid

Pi – Inorganic phosphate

mmol/gDW/h – millimoles per gram dry weight per hour

kNN – k-nearest neighbours

QC – Quality control

lb = lower boundary

ub = upper boundary

PEA – Pathway enrichment analysis

DNA – Deoxyribonucleic acid

NAD^+ - Nicotinamide adenine dinucleotide (oxidized)

$NADP^+$ - Nicotinamide adenine dinucleotide (oxidized)

NAD^+ - Nicotinamide adenine dinucleotide (reduced)

BCAT – Branched-chain α-keto acid dehydrogenases

CVDs – Cardiovascular diseases.

COX – Cyclooxygenase

COX-1- Cyclooxygenase-1

COX-2 – Cyclooxygenase-2

PGE2 – Prostaglandin E2

PGD2 – Prostaglandin D2

PGI2 – Prostaglandin I2

LTB4 – Leukotriene B4

LTC4 – Leukotriene C4

TXA2 – Thromboxane A2

PGH2 – Prostaglandin H2

5-HPETE - 5-hydropeoxyeicosatetronoic acid

12-HPETE - 12-hydropeoxyeicosatetronoic acid

CAVS – Calcified aortic valve stenosis

AS – Aortic stenosis

CAD – Coronary artery diseases

MPG – Mean pressure gradient

AVA – Aortic valve area

ACSS2 – Acetyl-CoA synthethase enzyme 2

HIFs – Hypoxia inducible factors

SDH – Succinate dehydrogenase

Flux abbreviations and their respective cell compartments names are found on the website: http://bigg.ucsd.edu/

Acknowledgements

I would like to first and foremost, thank my instructors Óttar Rólfsson and Adrian Lopez. They have offered me not only exceptional guidance throughout the entire process of this thesis but also, stilled very important principles in related to academic research. In the initial part of my masters, Adrian was the person who guided me through the computational aspects of this project. This in turn, compelled me to pursue a more computer-science/data science academic route. Hence, the gained programming skill set I've acquired is thanks to him. Furthermore, the biological insights that has been essential in understanding if what I'm seeing on my screen makes any biological relevance at every stage of the project can be all credited to Óttar. It goes without saying, thank you both.

Notable mentions go to friends that have accompanied throughout this journey. Arnar Ingi a member of our unhinged lab group, thank you for the data and all the support you've given specially in the last 2 weeks of writing this thesis. Eva Jacobsen, another member of the lab group. Thank you for tolerating the unhinged moments. I would like to express my sincerest gratitude to Tinna Björg and Maria Rose for the countless late nights spent together. The conversations, camaraderie, and the companionship you two have provided will always be cherished. In addition, I want to say thank you to Teitur Sævarsson, Perla Daníelsdóttir and Birta Dröfn for the companionship during my masters and the tons of laughs along with it. Lastly, a special mention to Hafdís María. She has been an outstanding moral support to me, a great friend through and through since my bachelor years and for that, I thank you, wholeheartedly.

This last portion of acknowledgment will be dedicated to my life-partner, Halldór Bjarni Stefánsson. Your insurmountable support and unconditional love for the past 9 years is deeply appreciated. Thank you so-so much Halldór.

1 Introduction

1.1 The endothelium and its role in blood hemostasis

During rest, the human cardiovascular system coordinated by rhythmic contractions of the heart, pumps 5-6 liters of blood per minute throughout the body, a rate that increases up to 5-fold during exercise[1]. One component of this system is the vascular endothelium, a monolayer of endothelial cells (ECs) forming the critical interface between blood and the vessel wall. A constant exposure to varying magnitude of mechanical forces such as shear stress (SS) are exerted to ECs due to blood flow. These forces are not only being withstood by the ECs, they are transduced into different types of biological responses through a process called mechanotransduction[2,3]. Mechanotransduction transforms mechanical stimuli into extra and intracellular signals that influences morphology, physiology, proliferation, adherence, and migration of ECs[4].

The blood flow-induced mechanical stresses on the ECs have been implicated to have an important role in the pathogenesis of several vascular diseases beyond the more common atherosclerosis, such as hypertension, vascular inflammation, and venous thrombosis[4]. Moreover, the flow patterns characterized by enhanced oxidative stress, inflammation, and even atypical adhesion of molecules have been shown to initiate and contribute to a variety of other vascular dysfunctions. These conditions not only exacerbate atherosclerosis by promoting a pro-inflammatory in ECs, but also impact in pact other aspects of vascular health[5,6]. In the case of hypertension, the continuous increase of blood pressure creates too much SS on the ECs, leading to destruction of the balance between vasodilators and vasoconstrictors, which would cause vascular remodeling and injury of the endothelium. Similarly, in low-flow venous thrombosis conditions, these hemodynamic states lead to endothelial activation, which participates in a pivotal role in the formation of a thrombus. Thus, these examples highlight the inherent relationship between the changes in behavior of endothelial cells caused by modified hemodynamic conditions and progress in several flow-related diseases[3–6].

One of the ways the endothelium can sense varying flow conditions is through the endothelial mechanosensors glycocalyx (GCX) and primary cilia. They serve as the major participants in facilitating the mechanical strain imposed onto ECs[2]. In the pathology of a rather prevalent disease in western societies atherosclerosis (and many other EC related diseases), both mechanosensors are affected[7,8]. Understanding how these structural components are degraded using enzymes to specifically target them can elucidate the key roles, they play in regulating vascular tone, cytoskeletal conformational changes, nitric oxide (NO) production, and their athero-protective properties in regions with disturbed flow[9–12].

The GCX is crucial for healthy vascular growth and function[13]. It is primarily composed of dense mesh of proteoglycans (PGs) equipped with glycosaminoglycans (GAGs) side chains and glycoproteins. This sophisticated structured network not only acts as a physical barrier safeguarding against unwanted cellular and macromolecular interactions but also actively

participates in mechanotransduction which promotes the ECs adaptive response to varying hemodynamic forces[2,3,14]. Experimental insights reveal that alterations in GCX constituents hyaluronan (HA), and syndecans induced by enzymatic degradation or high-oxidative-stress conditions can significantly impact EC remodeling, vascular tone, and homeostasis through regulation of NO[10,15,16].

Being one of the basic bases for vascular homeostasis and one also associated with the pathogenicity in conditions such as atherosclerosis, the role of the primary cilium towards mechanotransduction is vital[17]. Primary cilia are non-motile microtubule-based structure protruding from the surface of ECs (and many other vertebrate cells)[18]. Mechanistic studies have established that the deflection of primary cilia under SS triggers an influx of intracellular calcium through mechanosensitive channels, primarily polycystins 1 and 2 (PKD1 and PKD2)[19,20]. These channels are expressed on the primary cilium and have been linked as the initiation place for the cellular response to mechanical stimuli. Moreover, primary cilia gain significant importance as mediators in the development processes and disease pathologies relevant to endothelial vascular biology[21]. The general literature relevant to signaling cilia abnormalities is a part of a spectrum of pathological conditions that involves abnormal valvulogenesis and malformation of the otolith which underlines the role of primary cilia in signaling for development[2,22,23]. In regions with varying SS, studies done on the dynamic nature of the primary cilia elucidates that they were either maintained or reassembled further emphasizing their role in the development of atherosclerotic lesions[17]. This observation is consistent with studies where that ablation of EC dramatically worsens atherosclerosis which suggests that genes under control of primary cilia, are related to the suppression of genes involved in inflammatory gene expression and with endothelial NO synthase (eNOS) activity[21,24]. On the other hand, high SS is normally athero-protective and would predispose for the disassembly of primary cilia, indicating their selective localization to environments prone to vascular biology[25].

1.2 Changes to metabolism are linked to endothelial dysfunction.

The broader roles of ECs extend beyond just mere physical barriers. They are dynamic and energetic regulators of vascular development, angiogenesis, and contribute to the maintenance of metabolic homeostasis at both whole-body and local-tissue environment levels[26,27]. This outlines one of the major values in the metabolic plasticity of ECs: it enables adaptation by metabolic processes into a complex network from diverse physiological and pathological stimuli[28]. Such flexibility means that ECs can break off their traditional roles, which grants them a crucial place for regulation in vascular and metabolic balance[27].

Once thought to serve as little more than a basic wall, separating blood from the peripheral tissues, the interface between blood and vessel walls emerges as an actively participating filter in maintenance of vascular and metabolic homeostasis[29]. ECs respond to a series of metabolic stresses, many of which are triggered by hyperlipidemia and hyperglycemia[26]. However, this type of adaptation may lead to a state termed endothelial dysfunction, which contributes to the multifaceted development of diseases such as atherosclerosis, arterial hypertension and diabetes mellitus[27,30]. This transition from a quiescent to an activated dysfunctional state of the ECs represents not only their key role in healthy endothelial function and disease but also mirrors the complexity displayed by metabolic regulation and

vascular pathology[28]. This points to the importance of the endothelial metabolic plasticity in the wide setting of vascular biology and disease control[31].

Emerging research have shed light on the critical roles of endothelial metabolism and signaling pathways, namely several aspects of endothelial metabolism with respect to synthesis and regulation of NO, angiogenesis mechanisms, adenosine triphosphate (ATP) generation, glycolysis, fatty acids (FA) and lipids, metabolism of important nutrients, and signaling molecules[26–28,32,33]. These critical functions contributing to EC metabolism will be discussed and in the context of EC vascular pathologies. This diversified and specialized feature of the ECs metabolic repertoire reflect their critical importance in the biology of the vasculature. These are well equipped to satisfy the dynamic requirements of the vascular system, including the synthesis of NO and modulation of the angiogenic pathway, production of ATP, metabolism of glutamine, glutamate, FAs, lipids, and amino acids. This metabolic flexibility enables ECs to meet the metabolic requirements of respective local and systemic changes required to support essential roles in development and homeostasis, furthering the robust and plastic responses of the vasculature to injury. Insight into how ECs play a crucial role in supporting the metabolic balance of not only the vasculature and overall systemic metabolism, can best be obtained with understanding of the metabolic pathways occurring within the ECs. In the following sections, known metabolic dependencies of endothelial function are reviewed.

1.2.1 ATP generation and the predominance of glycolysis in endothelial cells

In spite of direct exposure to an elevated level of oxygen, the unique metabolic profile of EC highly prefers glycolysis against oxidative phosphorylation (OXPHOS) for generating ATP. The preference of glycolysis is clearly demonstrated during the metabolic processing of glucose, as most of it is metabolized to lactate, with only a little part of glucose actually being utilized in the tricarboxylic acid (TCA) cycle[27,34]. For example, in rat coronary microvascular ECs, glucose uptake is almost completely converted into lactate while it contribution to OXPHOS is minimal[35]. This metabolic trait is in apparent contradiction with the large mitochondrial volume inside ECs, pointing at an evolutionary specialization to carry out other cellular functions than those concerned with energy production[28,32,36].

Moreover, though the net ATP production by one molecule of glucose is lower than that of OXPHOS, the fact that ECs depend on glycolysis brings forward several physiological benefits[34]. Firstly, it extends the supply of lactate, which is an additional source of pro-angiogenic signaling. Second, it would reduce the generation of reactive oxygen species (ROS) that are usually generated under OXPHOS and hence reduce oxidative stress in ECs. Third, it would ensure this way that maximal reserve of oxygen is taken to be transferred to the surrounding tissues, which is an important function of the ECs. Moreover, the preference for glycolysis enables ECs to effectively function in the hypoxic condition prevailing in avascular/ischemic environments where sprouting of new vessels may arise[28,34,37–40]. This metabolic adaptation has special implications for quick ATP production and supports macronutrient synthesis that is required by the very high levels of cell proliferation and migration associated with angiogenesis[37,41,42].

Additionally, this glycolytic preference was shown to support the fundamental control of the EC in regulating the endothelial glycocalyx layer (EGL), known as another key constituent of vessel health through facilitation of mechanical forces[7,8,12,43]. This represents the high glycolytic fluxes needed in intermediate synthesis, such as the uridine diphosphates (UDP)

-glucosamine and UDP-glucuronic acid which are vital for EGL component biosynthesis[44]. Lastly, the modulation of glycolysis by SS-responsive elements includes Krüppel-like factor 2 (KLF2) in the determination of the thickness of EGL and its integrity. KLF2 regulates the EC metabolic pathways under both laminar and disturbed flow conditions, providing a direct linkage of glycolytic metabolism to dynamically regulated GCX[44,45].

1.2.2 Branched-chain amino acids, glutamine, and glutamate: their impact on vascular health and endothelial metabolism

Branched-chain amino acids (BCAAs) are essential amino acids (AAs) which include valine, leucine, and isoleucine[46]. They regulate and contribute to protein synthesis in muscles and other tissues[27,28,46]. These AAs are not only vital for the maintenance of skeletal muscle, but also for their influence on glucose metabolism and brain function, which, makes it as one of the common supplements in mental and physical performance enhancement[47,48]. Emerging research has suggested that BCAAs might be involved in vascular dysfunction through the pathways implicating chronic low-grade inflammation and oxidative stress, both centralized to type 2 diabetes (T2DM), obesity, and atherosclerosis pathogenesis[47,49,50]. The inflammatory processes stimulated by the BCAA-induced production of ROS, may damage the bioactivity of NO in the endothelium and probably induce more pro-inflammatory properties[46]. In addition, BCAAs are also involved in the signal processing of the metabolism and EC functions which affects migration and proliferation processes[46].

In parallel, glutamine and glutamate are AAs that are vital for EC metabolism[27,28]. Glutamate is the predominant AA in the intracellular environment in contrast to glutamine which is among the most abundant AAs in the extracellular environment under normal conditions[51]. However, glutamine requirements turn conditionally essential, usually under some stressed conditions such as trauma or intensive cancer therapies. The glutamine and glutamate (classified as non-essential AAs), remain vital for the support of EC function, owing to their highly oxidized states even under glucose-deprived conditions, signifying their importance to EC metabolism[52,53]. This is through the functions of glutamine serving as a nitrogen buffer/reserve and source of carbon for the TCA cycle in ECs, on a par with the contributions from glycolysis and fatty acid oxidation (FAO)[30,54].

The conversion of glutamine to glutamate is one of the major steps in the metabolic processing of glutamine, where glutamate is further catabolized directly to α-ketoglutarate[52]. This pathway guarantees ATP production, but above all, it grants the possibility that the anaplerotic reaction may supply intermediates to the TCA cycle[54]. Moreover, nitrogen deriving from glutamine assumes a very important role in the synthesis of nucleotides which highlights their contribution to the mechanisms of cell proliferation and repair[54]. Glutamine also supports the synthesis of asparagine, yet another important AA for the vessel sprouting[55]. Expanding its role in metabolic flexibility and support of ECs biosynthetic demands during vascular growth and repair. It is therefore assumed that glutamine and glutamate metabolism in ECs seem indispensable to the buildup of their energy production, biosynthetic capacity, and functional response in physiological or pathological angiogenesis[31].

In addition to changes in BCAAs and glutamine and glutamate metabolism, changes in tryptophan metabolism are observed together with endothelial dysfunction[56,57]. The biomarkers kynurenine and 5-methoxytryptophan (5-MTP) are indicated as very important

changes of metabolic routes that are crucial to cardiovascular health[57–60]. Kynurenine is one of the major products resulting from tryptophan catabolism; it helps in the regulation of immune homeostasis, modulation of inflammatory responses, and influences cellular proliferation[58,59]. Higher levels of kynurenine have been related to such an increased risk of acute myocardial infarction and accelerated progression of atherosclerotic changes, in particular among these patients, with disturbances of metabolism, such as diabetes [56,58,61,62]. 5-MTP, synthesized from L-tryptophan through a different pathway, mainly plays a role in the reduction of inflammation and associated endothelial barrier integrity through the p38 MAPK pathway[57,60,63,64]. Both metabolites, kynurenine and 5-MTP, significantly contribute to the understanding of metabolic functions in context to vascular health.

1.2.3 The critical role of fatty acid oxidation in endothelial cell proliferation and vascular integrity

Distinctly from other cell types, FA and lipid metabolism in ECs carry out critically different roles. Specifically, in the context of energy production and nucleotide synthesis for cell proliferation[28]. Proliferating ECs, therefore, become more dependent on FAO for continued nucleotide synthesis, even though it is not directly replenishing the TCA cycle in direct contrast to the canonical dependence on anaplerosis for the replenishment of TCA cycle intermediates[65]. This metabolic strategy has two implications; on the one side, fatty acid derived acetyl-CoA (coenzyme A) does not contribute toward net oxaloacetate (OAA) formation under conditions of sufficient anaplerotic substrates[28,65,66]. For example, glucose and glutamine. On the other side however, contribution has to be enough for TCA cycle functionality and its support for deoxynucleotide triphosphate (dNTP) synthesis which is essential for the proliferation of ECs[67].

A study where inhibition of carnitine palmitoyltransferase 1a (CPT1a), an enzyme key to the regulation of FAO, led to a reduced availability of the pool to replenish the TCA cycle intermediates and nucleotide precursors[65,68]. This decreased availability of metabolites indicates the roles of FAO in acetyl-CoA provision, acting in concert with anaplerotic substrates to maintain the TCA cycle and dNTP synthesis[65,67,69]. These EC metabolic insights underline the significant role of FAO in endothelial proliferation and indicate, specifically, how glucose and glutamine metabolism may be indispensable for maintenance but not compensatory for the absence of FAO activity[70]. Moreover, FAO contributes to the generation of nicotinamide adenine dinucleotide phosphate (NADPH), a cofactor crucial for maintaining cellular redox balance[71]. The oxidative TCA cycle, fueled by FAO, facilitates production of NADPH that further supports another step of the important antioxidant, i.e., the conversion of oxidized to reduced glutathione[71]. These functionalities highlight that ECs in their quiescent states have the ability to engage in activating an overall metabolic program to enhance NADPH synthesis for sustaining redox homeostasis among other pivotal functions for vascular protection. Thus, disordered FAO pathway mediated through CPT1a brings into the picture the role of this enzyme in EC dysfunction and increased vascular permeability through the induction of oxidative stress[65,67,68,72].

The lipid sphingosine 1-phosphate (S1P) represents as one of the most important elements that help in maintaining vascular integrity in ECs[73,74]. Emerging as a pivotal lipid mediator that participates in vascular dilation, permeability, cellular proliferation through migration and wound healings[73,74]. An established role of S1P is through its capability of reinforcing the endothelial barrier properties by regulating inflammation[75]. These effects are mediated by specific G-protein-coupled receptors (GPCRs) encoded by endothelial differentiation

genes (EDGs) that initiate signal transduction pathways critical for those endothelial functions, including cell migration, proliferation, and enhancement of the barrier[75,76]. In vitro studies have demonstrated that S1P stimulates the closure of wounded monolayers of endothelial cells, which is critical in wound healing through an increase in cellular migration and proliferation[74–76].

1.2.4 Vasoregulation is regulated by endothelial nitric oxide synthase

NO is synthesized by eNOS; this is one of the most important regulators of vascular health that greatly contributes to the maintenance of the vascular tone through several mechanisms, including the inhibition of aggregation in platelets and proliferation of smooth muscle cells[26]. eNOS activity, through a phosphorylation cascade and the entry of calcium, allows the finely regulated production of NO for rapid response by the endothelium toward a variety of conditions, including altered SS and hypoxic settings[77–79]. In addition, it mediates the synthesis of eNOS, which is responsible for the constitutive release in ECs, and it is also very essential in maintaining the homeostasis of the cardiovascular system. It modulates the tonicity of the vasomotion, ensures vascular integrity, and offers protection to the cells[80].

1.3 Exploration of the cellular metabolism through genome-scale metabolic models

Genome-scale metabolic models (GEMs) are integrated computational frameworks developed with the intent of being used for simulation and analysis of the metabolic capabilities of an organism at a genome level[81]. They account for all the metabolic reactions of an organism and the corresponding genes that encode the enzymes catalyzing these reactions. The crux of GEMs is the network representation of the metabolism, where nodes usually represent the metabolites, and edges correspond to the biochemistry reactions that link these metabolites[82]. This captures the metabolic pathways that are needed for life in the cell, from energy production to biosynthesis of other constituent parts of the cell.

The construction of GEMs starts from careful annotation of the genome and identification of genes associated with metabolic functions. The genomic information integrates with large amounts of biochemical data to build up a list of enzymatic reactions. Each of the reactions is described with quantitative directionality and compartmentalization within the cell. Thus, the model represents a metabolic potential for the organism under study[83].

Among the important features of GEMs are that they are modular in the integration of several types of omics data, from transcriptomics to proteomics and metabolomics. Such integration further makes it possible to refine the model in capturing the metabolic state of the organism under different environmental conditions or genetic perturbations[84]. Their applicability ranges from predicting cellular responses to changes in nutrition, genetic modifications, and exposure to drugs, hence providing insight into genotype-phenotype relationships[85]. However, it is paramount to acknowledge that, despite the wealth of data that can be harnessed, the inherent predictive nature of GEMs is bounded by the necessity of empirical validation[86]. Absent of such validation, the inferences drawn from these models retain their hypothetical status. A critical step of validation is to ensure that the model reflects biological accuracy.

1.3.1 Reconstruction using human metabolic models

The BiGG Models provide a method for the reconstruction and application of GEMs in a standardized platform toward the comprehension of the metabolic network in many organisms. The platform, designed as a comprehensive knowledge base of Biochemical, Genetic, and Genomic (BiGG), hosts over 75 manually-curated GEMs available for browsing, searching, and visualization[87]. One feature of BiGG Models is the standardization of reaction and metabolite identifiers in all models so that it was easier to ensure consistency during model development while also facilitating comparative analyses. This standardization is complemented by direct connection to model components with genome annotations and external databases. Additionaly, BiGG Models supports diverse applications in metabolic engineering, phenotype prediction, and the contextualization of omics data, offering tools for both visualization and detailed analysis (http://bigg.ucsd.edu/).

A major advancement in the progress of studying the complexities of the human metabolism through GEMS have been the amalgamation of comprehensive human metabolic models such as HUMAN1 and Recon3D[88,89]. The integration of numerous sources, including Human Metabolic Reaction 2 (HMR2), improved reconstruction of human metabolism (iHsa), and Recon3D, helped HUMAN1 provide a strong foundation for the representation of human metabolism at a genomic scale[88–91]. It further curates and integrates metabolic reactions with meticulously to avoid over-redundancy and feature inconsistencies, to make sure that the biological information is relevant and useful. Recon3D builds from this by populating it with the pharmacogenomic data and structurally providing a 3D view into metabolism. This is also integrated with the function to delineate how the variation affects the genetic changes and changes in protein structure that the metabolic pathways and phenotype change, resulting in the disease[89].

Following the development of comprehensive GEMs, the web application Escher represents as a significant tool in the field of biological pathway visualization[92]. Escher enables the further use of these models to rapidly build of biochemically accurate pathway maps help better understand the complex inter-relationships within cellular processes and their wider biological consequences. This is supported by the ease of integrating different datasets ranging from genes to reactions to metabolites, both within and across metabolic processes, in a manner facilitated through features such as clear visualization representation, map design customization, and ease of navigation. Additionally, Escher gains benefits from being a web application such as immediate setup, cross-platform compatibility, and simplified sharing and collaboration. Escher is also characterized by semi-automatic map construction, using existing data and models in suggesting pathways, view of genomic data on reaction networks, and integrations of detailed information on biochemical reactions and genes[92,93].

1.3.2 Context-specific models are able to capture the dynamic landscape of cellular metabolism

Context-specific GEMs are specialized versions of generic GEMs that have been constructed to reflect the unique metabolic activity, characteristic of a certain cell type or tissue[94,95]. These quantitative dynamic models are formulated by integrating diverse 'omics' data with an organism-specific comprehensive metabolic model that includes all known reactions and associated genes[96]. The major goal of context-specific GEMs is the refinement of broad models that will help capture the an accurate metabolic state of a cell under specific condition

or environment[97]. In this regard, it will be possible to associate the changes in gene expression or protein levels to the metabolic pathways and cellular phenotypes directly[96,97].

The rFASTCORMICS algorithm implemented in this domain is designed explicitly for the rapid and accurate construction of high-resolution, context-specific metabolic models[98]. rFASTCORMICS first introduced for microarray data and later adapted to RNA-seq data can fully outline metabolic networks in cancer cells, allowing the opportunity to study the strategies of metabolic rewiring crucial for the understanding of cancer metabolism[98,99]. It is aimed at identifying and categorizing metabolic reactions from based from transcriptomic data into core, non-core, and inactive sets. The algorithm then builds a context-specific model by including only those reactions that are predicted to be active based on available gene expression and pre-defined gene-protein-reaction (GPR) rules. Furthermore, since it does not require optimization targeting a product like biomass, rFASTCORMICS is also amenable to building models of non-proliferative cells, a great advantage in the study of many cellular conditions[98]. In cancer-specific studies, rFASTCORMICS is able to show lilely metabolic liabilities and therapeutic targets from a comparative analysis of metabolic pathways that exhibit difference between normal and cancerous tissues[98–100].

Gene Inactivity Moderated by Metabolism and Expression (GIMME) and Integrative Metabolic Analysis Tool (iMAT) are two computational tools that generates context-specific GEMs that we considered for this study[101,102]. GIMME has been succesfuly applied to the adaptive evolution of bacetria, metabolic engineering, and analysis of human skeletal muscle cells[101,103,104]. iMAT on the other hand, has been used to predict metabolic fluxes through bypassing assumptions about metabolic functionalities of particular network which can be succesful for context-specific GEMs with no clear objective function to maximize such as mammalian models[102,105].

The Constraint-Based Reconstruction and Analysis (COBRA) framework is used to integrate experimental molecular systems biology data with computational modeling to predict physiologically feasible phenotypic states[106]. COBRA uses a stoichiometric matrix that describes the mass-balanced metabolic reactions and substrate uptake and production rates that account for the mapping of changes of levels of reactants and products for each reaction[107]. COBRA effectively reduces this large, potential solution space by applying a series of constraints such as mass conservation, steady-state conditions, and defined flux boundaries to a more manageable 'flux cone' of feasible flux distributions[106]. These constraints are important to understand the molecular influence of both genetic and environmental factors on the cellular phenotypes[108]. Further refinements with constraints on enzyme capacities, metabolite availability, thermodynamics direction, space compartmentalization, and regulatory mechanisms, bring context-specific GEMs to becoming more predictive and of great biological relevance[106,107,109].

In this framework, Flux Balance Analysis (FBA) is a mathematical approach that calculates the flow of metabolites through the metabolic network in steady-state, where the level of internal metabolites does not change with time[105,110]. FBA seeks to maximize a specific objective function, such as biomass function, which is used as a surrogate for cellular growth, while imposing constraints in the form of mass balance and thermodynamic feasibility. However, FBA has the potential to yield multiple or undefined solutions which led to the development of Flux Variability Analysis (FVA)[111,112]. It is a method of characterizing the potential range of flux for each reaction and, in the process, an expanded view of the metabolic capabilities over conventional FBA. Furthermore, parsimonious Flux Balance Analysis (pFBA) offers another solution by finding the most efficient metabolic pathways

that requires the least enzymatic effort[113]. This approach adheres to the principle of "minimal resource utilization" and is particularly insightful for determining the metabolic strategies used by organisms under varied growth/resource conditions.

Of particular interest in the COBRA framework is the application of an advanced method named optGpSampler[114]. The method enhances exploration towards feasible flux distributions in high-dimensional metabolic networks by employing a modified Hit-and-Run (H&R) algorithm that can optimally bound complex solution spaces[115]. The sampling process starts at random initial points corresponding to the flux cone within the feasible solution space. The points are yielded by solving linear programming problems that minimize and maximize each reaction flux under the constraints of the model. These points yield an initial sampling within the flux cone[114,115]. After this process, Artificial Centering Hit-and-Run (ACHR) is used to readjust the direction of the sampling by focusing it on the less explored area of the solution space so that a more balanced distribution of the sampling is derived[116]. Finally, the optGpSampler may be parallelized since it starts multiple independent sampling chains at the same time, thereby increasing computational efficiency. This parallel processing decreases the total computational time and, therefore, does result in improvement over scale for the sample flux distribution. When aggregated, samples from all chains offers a comprehensive and statistically significant portryal of feasible metabolic flux states under multiple physiological conditions[114].

Advancement in creating high-resolution context-specific GEMs will be paramount to further the understanding of cellular metabolism. They will allow for the study of metabolic activities at a resolution that will reflect the unique biological context of a specific cell types or tissues. Hence, increasing the scope of prediction and application of metabolic models both in basic research and clinical studies[84,95]. In practical terms, GEMs have demonstrated their potential to pinpoint metabolic dysfunctions of humans concerning numerous diseases, suggesting possible therapeutic targets. For example, context-specific GEMs have been shown to be highly informative about metabolic alterations in diseases such as liver and breast cancers, as well as acute conditions such as sepsis and viral infections[95]. One of such applications has been to the GEM of human endothelium, iEC2812, for an analysis of metabolic reprogramming in sepsis through integration with transcriptomic data. This was important to unravel the metabolic changes in endothelial cells and their role in causing endothelial dysfunction—a major determinant of the outcome of sepsis[117]. In another development, using the case of hepatocellular carcinoma, one of the most lethal forms of liver cancer, task-driven model reconstruction algorithm (tINIT) was applied that integrated GEMs with gene expression data and network analysis to help identify non-toxic metabolic targets whose perturbation may be effective in killing cancer cells[118,119]. The development of GEMs underline the transformational impact of high-resolution GEMs in unraveling of complicated disease states and the pursuit of targeted medical strategies[95].

1.4 Aims

In this study we sought to better understand the metabolic perturbations that occurs in ECs under different flow conditions. That is, laminar, oscillatory, and static (lack-of flow). To achieve this, our aims can be developed into the following:

1. Develop a pipeline that would take omics data, reconstruct context-specific GEMs, and give an output of predicted differential fluxes and the enriched pathways.

2. Construct GEMs using transcriptomic data and metabolomics data from samples that have been cultured in laminar, oscillatory, and static conditions.

3. Predict differential fluxes between oscillatory versus laminar and static versus laminar conditions.

4. Derive biological interpretations on the perturbed pathways observed in our differential flux comparisons.

2 Methodology

2.1 Cell culture set-up

Cell culture experiments were performed under supervision of Dr. Thomas Duflot at The University of Rouen, France. Briefly, human heart valvular ECs were isolated from three patients undergoing cardiac surgery and cultured in Endothelial Growth Medium 2 (EGM2) medium under static conditions, laminar flow at 20 dynes/cm2, and oscillatory flow at 20 dynes/cm2 using the ibidi pump system® (www.ibidi.com). EGM media was harvested from these experiments at 4h and 24h post seeding for metabolomics analysis. Ribonucleic acid (RNA) extraction was performed by phenol chloroform extraction. The details of these experiments were the subject of Ms. Margaux Marie Tanguy MS thesis that is available in French upon request. An overview of the experimental setup is shown in Figure 1 below, reproduced from Ms Tanguys thesis[120].

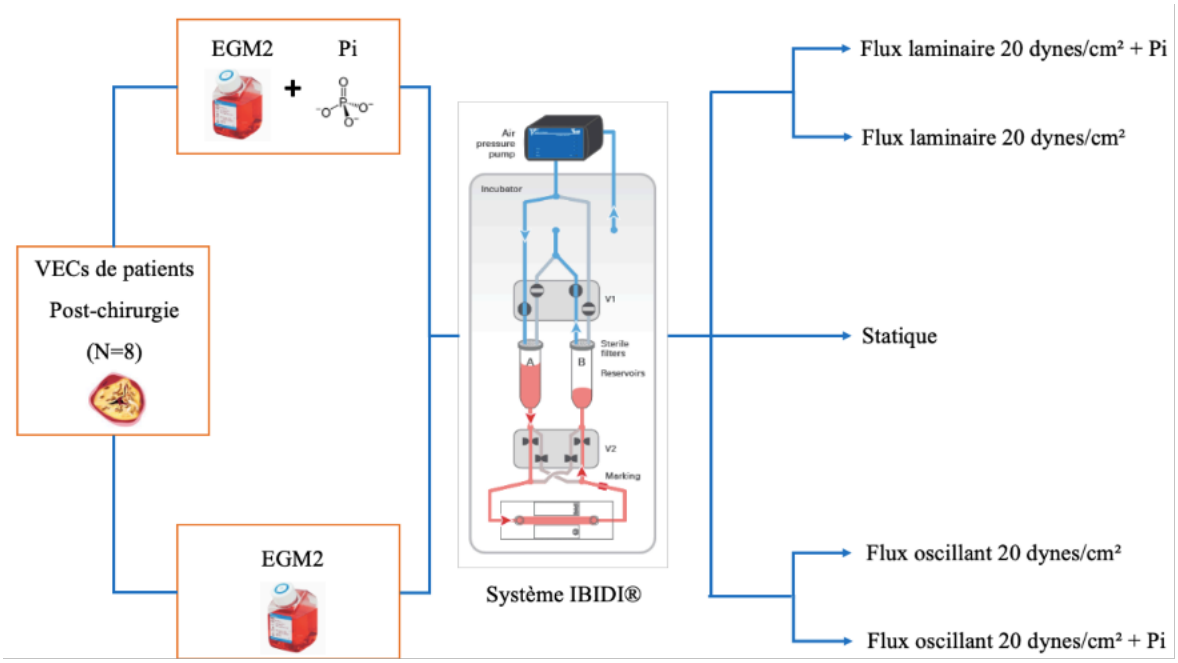

Figure 1 – Experimental design of the flow culture protocol of ECs from calcified valve samples. ECs were harvested from patients after surgery (n = 8). The cells are cultured in EGM2 and, optionally, with an inorganic phosphate (Pi) supplement under flow regimes, such as, laminar or oscillating flow and static conditions. The setup uses an IBIDI® system through a computer-controlled air pump that simulates in vivo shear stress conditions. It consists of a fluidic unit with an EGM2 medium reservoir—three µ-Slides linked to the latter by a closed tubing circuit—allowing for real-time monitoring and the control of the frequency and amplitude at which in vivo shear stress is simulated through a computer-driven air pump. In between, oscillating or laminar control of the fluid flow direction is offered by the electromagnets through electrically operated valves. The complete assembly is maintained in an incubator at 37°C in an atmosphere of 5% CO2 and humidity for 48 hours. The cells were then seeded a concentration of 100,000 cells/ml into the µ-Slides and grown overnight, statically, in an incubator at 37°C and 5% CO2. Cells from each patient are randomly allocated to one of five experimental groups: static, laminar flow (20 dynes/cm²) with or without Pi, and oscillating flow (20 dynes/cm²) with or without Pi.

2.2 RNA-sequencing data

Transcriptome profiles from three samples 154, 153 and 46 from the flow conditions laminar and oscillatory, and static conditions were used to build 3 models for analysis. Samples containing Pi were not of interest of study at this time and thus, were omitted for further analysis. There were other samples in the initial stage but due to their absence in other conditions, they were also omitted (*Table 1*).

*Table **1** – RNA-Seq data of the harvested ECs from calcified valve samples that have been cultured and subjected to laminar or oscillatory flow, and static conditions. Transcriptomic data highlighted green (154, 153, and 46) were used to build GEMs in our studies. Samples containing Pi were not the focus of the study at this time and were therefore, excluded from further analysis.*

Condition	Sample 1	Sample 2	Sample 3	Sample 4	Sample 5	Sample 6	Sample 7	Sample 8
Laminar	154	153	46	94	NA	NA	NA	NA
Laminar w/ Phosphate	154	153	46	94	109	176	NA	NA
Oscillatory	154	153	46	NA	109	NA	NA	NA
Oscillatory w/ Phosphate	154	153	46	NA	109	NA	178	175
Static	154	153	46	94	109	176	NA	NA

Therefore, the transcriptome profiles for samples 154, 153 and 46 serves as one of the three primary inputs to construct three distinct and representative GEMS that can encapsulate the nuanced metabolic shifts occurring under these varying mechanical stimuli.

2.3 Metabolomics data

Metabolomics data consisting of measured experimental uptake and secretion rates of 56 metabolites were used to further constrain the three GEMS. The EGM media where the cells grew were harvested at 4h and 24h time points (post-seeding). Having metabolomics data, the predictive power of a metabolic model greatly increases and be more reflective of the actual physiological state of the cell.

The measured uptake and secretion rates were initially in mmol/L, which were then converted to millimoles per gram dry weight per hour (mmol/gDW/h). This conversion was necessary to align the data with the modelling framework that operates on a per biomass basis, allowing for a more accurate representation of cellular metabolism relative to cell size and number. The conversion also facilitates direct comparisons with other studies that commonly use this unit. We had information that roughly 100,000 cells were subjected to media (consisting of 56 metabolites) for 48 hours. In addition, the value we used for the estimated cell dry weight of ECs is 0.9 ng, as taken from previous literature[121]. This leads us with a constant of 0.00432 that is then divided by each measured uptake and secretion rates. Lastly, we calculated the mean values from the three samples for each condition—laminar, oscillatory, and static—to obtain a single representative value for each of the 56 metabolites under different conditions.

A subset of metabolomics data was missing for sample 46 in static conditions. Therefore, we had to impute this missing data from other measured uptake rates (samples 154, 153, 94, 109, and 176) using k-nearest neighbours (kNN) from the function *KNNImputer* which is

from the package *sklearn.impute*[122] using the parameter *n_neighbours = 3*. This algorithm was selected for its ability to estimate missing values based on the similarity of data points in a multidimensional space. The nearest neighbors were chosen based on their closeness in the dataset, ensuring that the imputed values are in line with the trends observed in similar samples. To validate the imputed data for sample 46, we examined the behavior of other static data and concluded that the imputed data somewhat followed the same trend. This observation provided a level of confidence in the reliability of the imputed values and their consistency with the overall dataset trends. This step is crucial for maintaining the integrity of the model predictions and ensuring that the imputed values do not introduce significant biases or deviations from the observed biological phenomena.

Furthermore, measured uptake rates were incorporated in a different manner during model creation for this study. The usual approach in constraint-based modelling is to define a medium composition (in the form of *cvs* file or an *xlsx* file) consisting of metabolite identifier and their measured uptake or secretion rates in mmol/gDW/h units. However, when we performed quality control (QC) checks on our metabolomics data. We determined that secretion (positive) or uptake (negative) of the metabolites never crossed a +1/-1 for all metabolites. Hence, we instead modified the lower and upper boundaries of the 56 metabolites in the model. For example, at *Figure 2*, the fourth metabolite *Cystine.P*, the modification for the oscillatory model would be: lower boundary (lb) = 0 and upper boundary (ub) = 1. As for the static and laminar models, the modification would be lb = 0 and ub = -1. Lastly, this data also serves as two out of the three main inputs to create GEMs for each flow.

2.4 Reconstructing context-specific models using rFASTCORMICS

The workflow towards model creation follows a similar procedure to rFASTCORMICS example script provided in their GitHub repositories and was executed in MATLAB[98,123]. This begins with pruning the expression profiles of the three samples (154, 153, and 46). Initial units of the RNA-Seq data were in Fragments Per Kilobase Million (FPKM) to which we calculated the mean for three samples across one flow condition and this step was repeated for the other two flows. Resulting into one representing expression profile for each flow condition. Each transcriptome flow profile is then subjected to the *discretize* function which discretizes the genes into either expressed, unexpressed, and ambiguous or unknown expressed genes. Then, we loaded Recon3D to serve as not only the final primary inputs to model creation but also function as a base-model containing extensive human genome annotations that can be reconstructed into a GEM[89]. Following the rFASTCORMICS example script, we also employed the function *fastcc* for Recon3D instead of Recon 2.04[98,124].

Measured uptake and secretion rates of the 56 metabolites were incorporated through boundary modifications. Our metabolomics data was in the form of a *xlsx* file which consisted of 56 Recon3D metabolite identifiers and using this data we created three versions of the base-model Recon3D (after employing *fastcc*) for each flow. This results where each version, the upper and lower boundary of metabolites were modified accordingly.

To create three context-specific GEMs, we applied the function *fastcormics_RNAseq*. The parameters we set when we applied the function were similar to the example script. Lastly,

prior to random sampling, the biomass function of each of the laminar, static, and oscillatory context-specific GEMs were reduced by 90%.

2.5 Constraining metabolic fluxes

Metabolic flux predictions of the laminar, static, and oscillatory models was performed by using a version of statistical method of random sampling called *optGpSampler*[125]. During this process, we confined the models to only explore 90% of the biomass which was calculated using FBA[110]. The explorations for each model were iterated for *n_iteration = 1000* and then random sampling flux results were again pruned into one representative mean value for a given flux. (Note: Supplementary material containing the three models as well as their constrained versions are accessible through this google drive link.)

2.6 Statistical analysis and transformation

Prior to differential flux analysis, feature transformations we applied to the raw values from the random sampling for each model (4224 intersecting fluxes *n* and 1000+ random sampling iterations *m*) such as logarithmic scale transformation and handling special cases such as zero, positive, and small negative values.

- Log_2-fold transformation; a logarithmic transformation is often used in data analysis approaches to handle skewed data distributions, specifically when dealing with a wide range of values present in gene expression data. Alleviates the impact of very large values to make patterns in data discernible.

- Handling of zero values; if a flux value is found to be zero, leave it untouched at zero. This approach is used because logarithmic functions are undefined at zero and for practicality, a zero-flux value is retained. Typically in a RNA-Seq data, a zero value indicates that a particular gene (in this case, a metabolic flux) is not expressed in the sample being analyzed. Retaining these zero values as-is is crucial because they can carry meaningful biological information. If one would add a small constant before log transformation, this could erroneously implicate a gene expression when there is none.

- Handling of small positive values; Flux values that were between zero and two (very low values but not zero) were handled by adding a small constant and then transformed. This scales and shifts these flux values so that it ranges from zero to one. Applying direct logarithmic transformations of these would result in negative values which can be misleading in the context of RNA-Seq data.

- Handling of small negative values; In the case of having negative flux values, which normally, in RNA-Seq data is not present as they represent intensities or counts of a gene expression are inherently non-negative. They were handled by first converting them into positive values by calculating their absolute value, a similar logic to the small positive values is repeated, and then the negative sign is re-applied. A symmetrical treatment to negative values is then achieved as their magnitude is just as important as their counterpart.

Upon flux transformation, each *m* for a given flux *n* is then pruned into a singular value by taking their median. Moving forward, the laminar flow condition is treated as the "healthy" condition and both oscillatory flow and static conditions are then compared to laminar flow.

Median differences between conditions which will serve as the basis for the *y-axis* in the metabolic differential flux figures through subtraction of oscillatory/static *m* median values (treated) to laminar *m* median value (control). Then, a t-test and a p-value correction are subsequently performed to the pruned median values (not the median differences) where a Benjamini/Hochberg (non-negative) and *alpha = 0.05* was used.

(Note: the code developed to generate models, constraining, and perform differential flux analysis is available in my GitHub page)

3 Results

3.1 Uptake and secretion rates of metabolites characterizes *in vivo* endothelial cell environment

Integration of metabolomics data to GEMs bridges the link between genotype and the phenotype of an organism. These datasets offer insights into the cellular responses to genetic or environmental changes that can be useful in characterizing the response of behavior of the biological systems to different conditions. This is specifically relevant in constraining the exchange reactions in the model as it limits the range of possible fluxes through the network and understanding the distribution of metabolic fluxes to identify key metabolic pathways that are perturbed under specific conditions.

Before the boundary modifications, the lb and ub for the majority of the metabolites have a range from 0 to 1000, 0 to -1000, and -1000 to 1000. Therefore, despite not following the general approach, reducing the boundaries by a thousand already constrains the biological system by a lot in contrast to setting a specific uptake or secretion value. This paints a more realistic picture physiologically, of what happens in the system as the modification is in the form of a range and disregards the marginal standard deviations for the measured uptake and secretion rates of the metabolites.

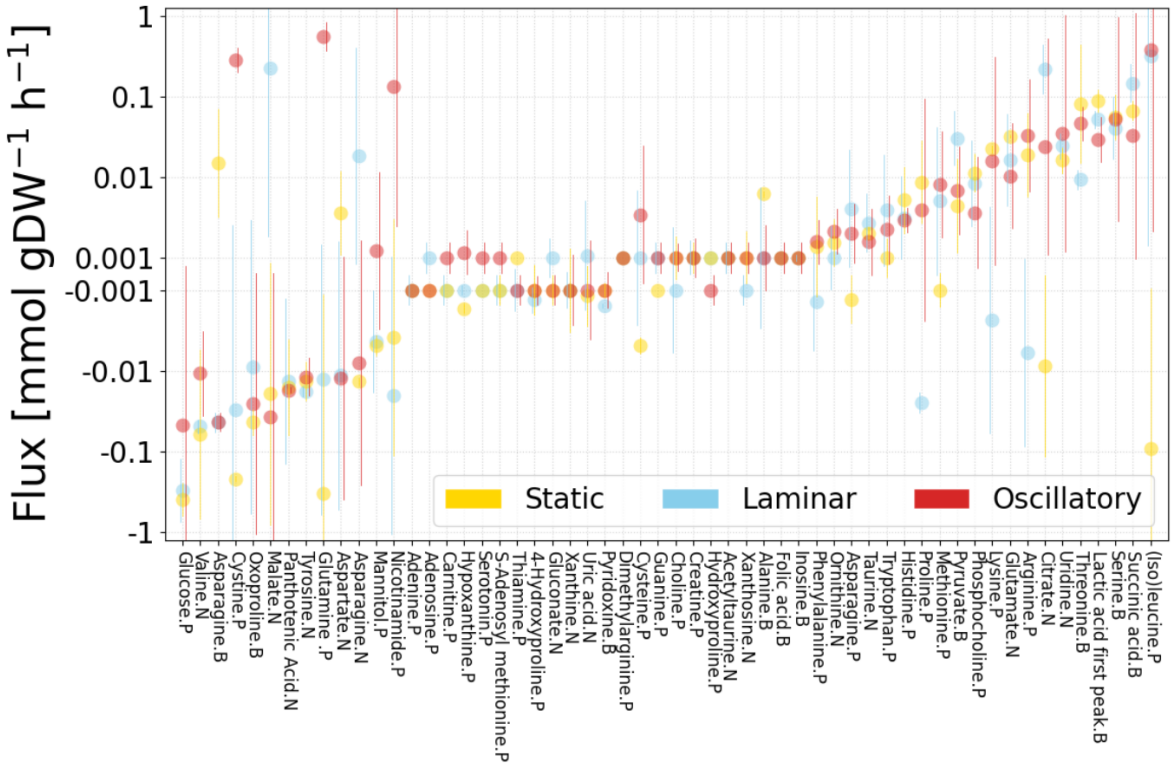

Figure 2 – Uptake and secretion rates of the 56 metabolites in the EGM2 media. This figure presents the experimental uptake and secretion rates of metabolites from ECs cultured under laminar and oscillatory flows, as well as static conditions. The 'P', 'B' and 'N' after each metabolite denotes the mode that the metabolite was detected in the mass spectrometry analysis and stands for positive, basic, and negative, respectively. Each dot represents the median rate for a metabolite across three samples (154, 153, and 46), with colors corresponding to the respective conditions: static (yellow), laminar (sky blue), and oscillatory (red). Standard deviations are indicated by the lines on each dot. The y-axis is divided, with negative values indicating metabolite uptake and positive values representing secretion. The position of each metabolite on this axis was used to establish boundary conditions for the respective conditions during the creation of our models.

3.2 Identification of differential metabolic fluxes across flow

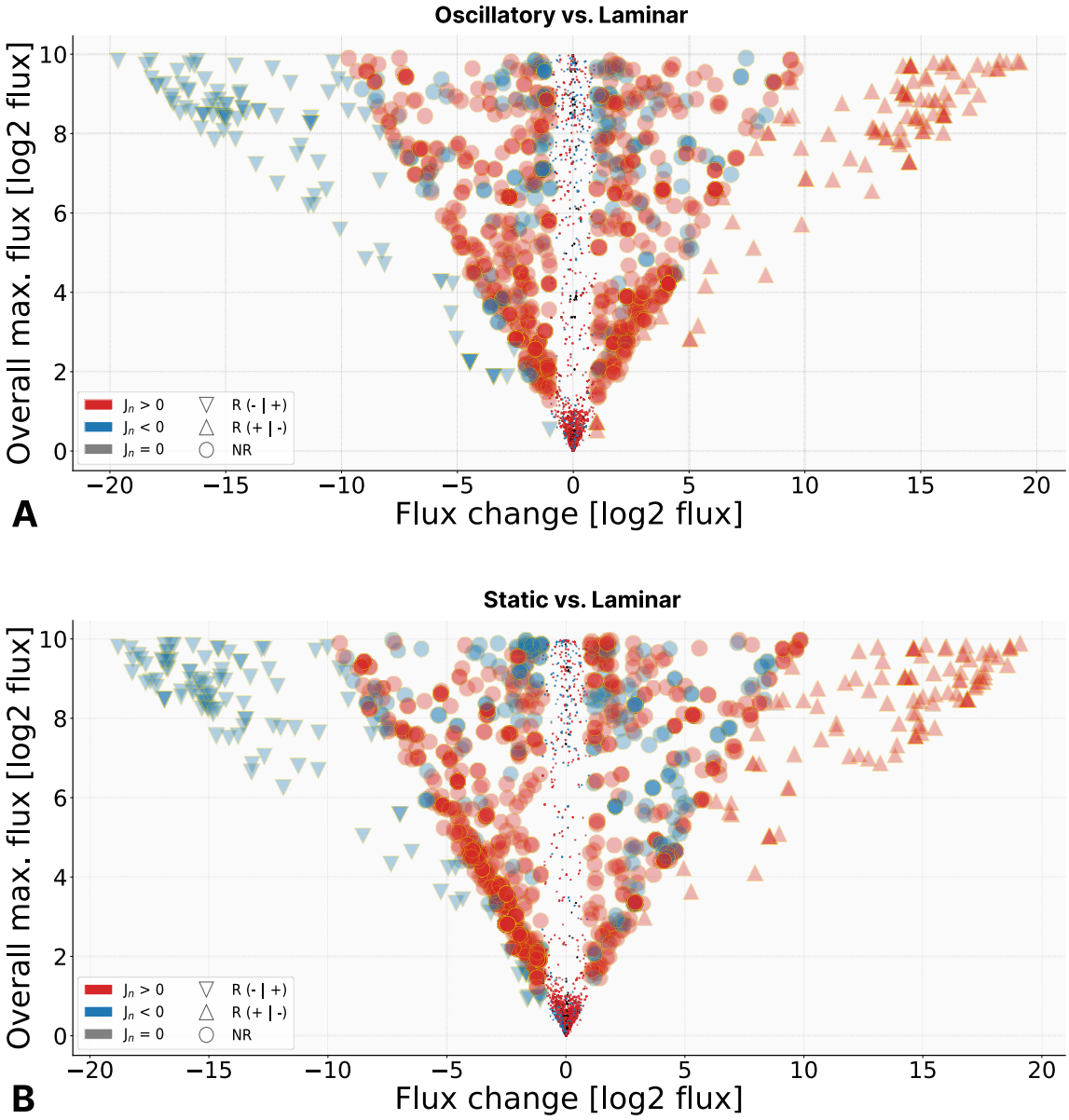

Figure 3 - Identified metabolic differential fluxes in (A). Oscillatory flow vs. Laminar flow and (B). Static condition vs. Laminar flow. Volcano plot of significant metabolic differential fluxes that passed a significance threshold log2-fold change of +1|-1. The legends represent different types of flux behaviour: the upside-down triangle R (-|+) indicates a flux that had negatively reversed in comparison to the control (originally a positive flux and reversed to a negative flux), the upright triangle R (+|-) indicates a positively reversed flux in comparison to the control (originally a negative flux and reversed to a positive flux), and the circle NR, subsequently, represents non-reversal fluxes.

Once our models have been reconstructed using rFASTCORMICS, Recon 3D, metabolomics, and transcriptomics data. We further constrained the 3 models using

optGpSampler to uniformly sample the predicted metabolic fluxes in our modesl confined to a solution space of 90% biomass to yield an unbiased portrayal of feasible metabolic fluxes across oscillatory, laminar, and static conditions. Predicted differential metabolic fluxes is then analyzed (*Figure 3*). The upper half (A). oscillatory versus laminar, there were a total of 950 metabolic fluxes that passed the threshold and 439 of those were positive fluxes (red) and 511 were negative (blue). The bottom-half (B). static versus laminar, consisting of a total 1117 fluxes, consisted of 456 positive and 661 negative fluxes (*Figure 3*). The fluxes in left are those fluxes that have decreased in comparison to control (laminar), points in the right are those fluxes that have increased in comparison to the control, and the colour determines if the fluxes are either negative or positive in the end of the comparison. Based on these results, we can discern that flow does indeed affect EC metabolism substantially. This implies that the models created, can capture the distinctive metabolic landscape under different conditions and further inferences can be made using these endothelial GEMs. (Note: Supplementary material containing predicted flux values that was used to build the volcano plot can be access through this google drive link.)

3.3 Pathway enrichment analysis reveal that five unique metabolic pathways are perturbed in flow

To better interpret and elucidate the implications of both the significant forward and reversed fluxes in *Figure 3*, pathway enrichment analysis (PEA) akin to hypergeometric geometric performed. Hypergeometric testing is a statistical procedure that can be used to test a significant number of successes in a sample compared to the number expected by chance; this test is often used when considering pathway enrichment analysis to show whether some biological pathways contain an overrepresentation of genes (fluxes in this case). Dataset containing the significant fluxes for the two comparisons as well as the *pre*-pre-processed dataset (immediately after flux transformation) were used for PEA. Here, a web-based tool Escher was used to aid in visualizing the resulting enriched metabolic pathways[92]. For consolidation, Recon 3D was loaded prior to mapping the set of significant fluxes and their $\log_2$-fold change values as well as those non-significant fluxes found in the total set to each pathway depicted below. (Note: Supplementary material containing detailed information's of the pathway enrichment analysis results can be accessed through this google drive link)

Table 2 - Pathway Enrichment Analysis Results. There were three enriched pathways in oscillatory vs. laminar and that is also shared of the five enriched pathways in static vs. laminar found in the analysis.

Pathway	p-value	Corrected p-value	Set	Total Set	Comparison
Eicosanoid metabolism	7.009E-08	3.180E-06	21	29	Oscillatory vs Laminar
Valine, leucine, and isoleucine metabolism	1.483E-05	3.37E-04	16	24	Oscillatory vs Laminar
Glutamate metabolism	1.198E-03	1.818E-02	6	7	Oscillatory vs Laminar
Valine, leucine, and isoleucine metabolism	2.165E-07	9.852E-06	19	24	Static vs Laminar
Citric acid cycle	1.109E-04	2.019E-03	12	16	Static vs Laminar
Eicosanoid metabolism	1.081E-04	2.019E-03	18	29	Static vs Laminar
Glutamate metabolism	2.239E-03	2.721E-02	6	7	Static vs Laminar
Arachidonic acid metabolism	2.992E-04	4.434E-03	9	11	Static vs Laminar

3.4 Shared perturbed metabolic pathways across conditions

3.4.1 Glutamine & glutamate metabolism fuels fluxes towards α-ketoglutarate

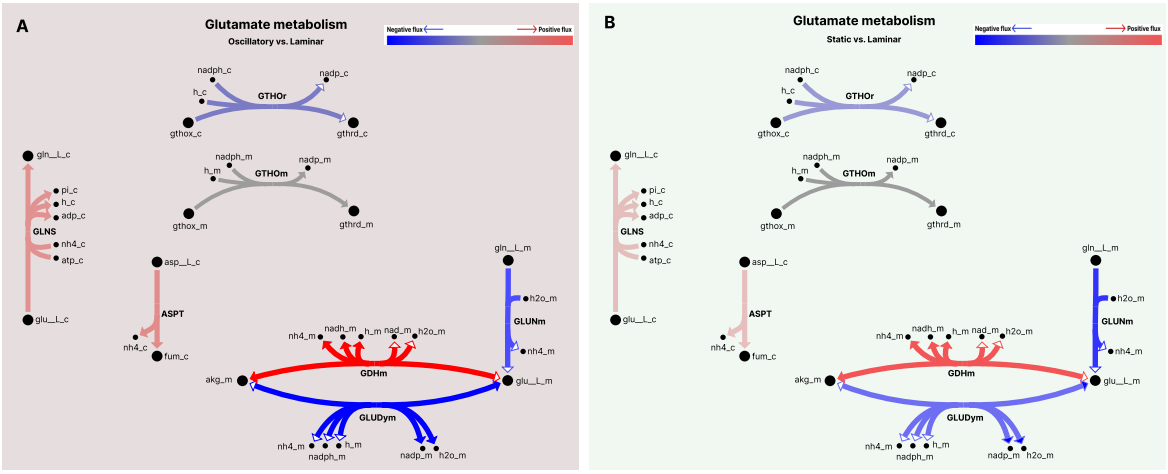

Figure 4 – Enriched pathway visualization of the glutamate metabolism in (A) Oscillatory vs. Laminar flow and (B) Static condition vs. Laminar flow using Escher. Our PEA results reveal that in both panels, 6 out of 7 fluxes were significant (refer to Table 2 for corrected p-value). These results are visually represented by colours: red indicates that the flux is positive, blue signifies that the flux is negative, and grey denotes non-significant fluxes. Variations in the shades of red and blue are used to depict the strength of each significant flux.

Glutamine, the most concentrated free AA in human plasma, and physiologically, an essential AA in cellular metabolism and physiology. Its relevance playing critical and diverse roles in supporting cell bioenergetics, contributing to protein synthesis and other macromolecule synthesis, and facilitating nitrogen transfer to build nucleotides for deoxyribonucleic acid (DNA) and RNA synthesis production[28,30,126]. The metabolism of glutamine begins with its conversion to glutamate and ammonia, a process catalyzed by glutaminase. Further metabolism of glutamate, which is an important carbon source used for TCA cycle replenishment, may go through an alternate pathway to furnish α-ketoglutarate or glutamine[51,52]. Moreover, the entering nitrogen from glutamate will be one of the very important molecules in the biosynthetic pathway of non-essential AAs. These are; proline, ornithine, and arginine, which are used for polyamine production and further transformed into NO. In addition to metabolic roles, glutamate also plays a role in enhancing glucose utilization, stimulate anti-inflammatory and immunomodulating responses, enhance glutathione synthesis, and support anabolic functions[53,127].

In visualization of the PEA results using Escher (*Figure 4)*, the glutamine and glutamate metabolism is one of the shared enriched pathways in comparing oscillatory and static differential fluxes to laminar. In addition, the overall fluxes in the pathway at both comparisons show a very similar behavior. That is, 6 out 7 of the significant fluxes found in the pathway are present except for glutathione oxidoreductase_m (*GTHOm*). From the 6 present significant fluxes glutamine synthetase (*GLNS*), aspartate ammonia-lyase (*ASPT*), and glutamate dehydrogenase_m NAD^+, (*GDHm*) are positive significant fluxes (filled arrows) and the rest glutathione oxidoreductase_r (*GTHOr*), glutaminase_m (*GLUNm*), and glutamate dehydrogenase_m $NADP^+$ (*GLUDym*) are negative significant fluxes (hollow arrows).

Fluxes *GDHm*, *GLUDym* and *GLUNm* altogether, show a strong inclination in catalyzing the conversion of glutamate into α-ketoglutarate whilst reducing the coenzymes NAD^+ to NADH and generating ammonium[126,128]. The effect of disturbed flow (oscillatory) or lack there-of (static) may implicate that in these flow conditions, the EC metabolism is trying to support the anaplerotic carbon donation to the TCA cycle and maintain redox balance against ROS[129]. Moreover, ammonium can be deaminated and act as a nitrogen donor to the TCA cycle and through carboxylation reduction, participate in FAO and lipid metabolism[127]. Through *ASPT* flux, ammonium concentration levels are further increased through the catalysis of the non-oxidizing elimination of ammonia from aspartate to generate fumarate and ammonia[130]. *GLNS* however, can regulate the nitrogen metabolism through conversion of free ammonium and glutamate into glutamine[53,131].

3.4.2 Perturbations on the valine, leucine, and isoleucine show their catabolism into succinyl-CoA

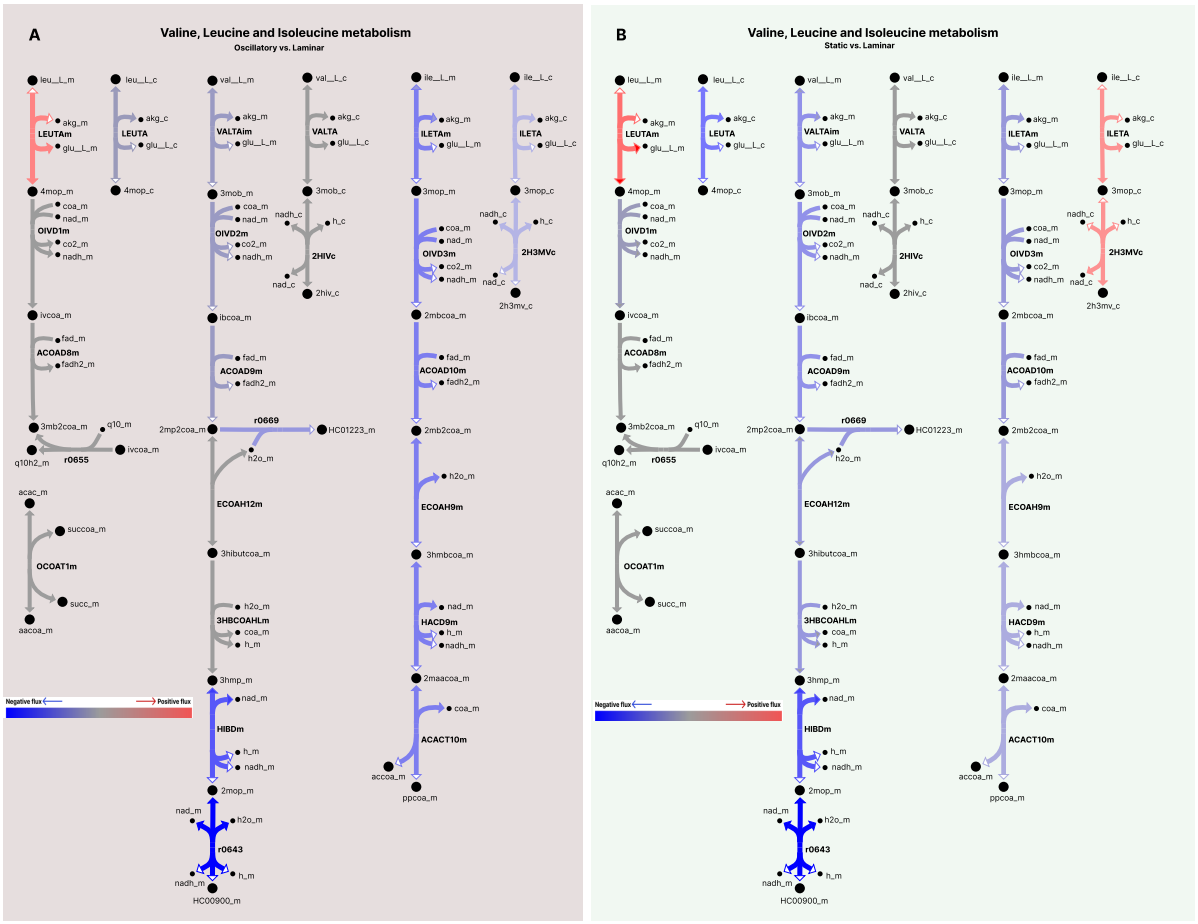

Figure 5 – Visualization of the enriched pathway for valine, leucine, and isoleucine comparing (A) Oscillatory vs. Laminar flow, and (B) Static condition vs Laminar flow. In (A), we observed 16 significant fluxes out of 24 in the total set and in the comparison for (B), 3 additional fluxes were identified tallying up to 19 significant fluxes out of 24 (refer to Table 2 for the corrected p-values). The rest of the pathway maps follows the same pattern as Figure 4 in relation to the colours.

During the catabolism of the BCAAs which occurs primarily in the skeletal muscles, they are first degraded into their respective keto acids after transamination. A second intermediate step is followed and is catalyzed by the enzyme complexes involving branched-chain α-keto acid dehydrogenases (BCAT). This irreversible decarboxylation of the BCAA keto acids leads to diverging pathways. The products of valine can lead to succinyl-CoA, leucine products can be further catabolized into acetyl-CoA or acetoacetate, and lastly, isoleucine by-products can either go to acetyl-CoA or succinyl-CoA[132–135].

The results of the PEA on the metabolism of valine, leucine, and isoleucine shows a consistent behavior in comparing oscillatory flow and static conditions to the laminar. Specifically, 16 significant fluxes out of 24 in the oscillatory versus laminar conditions and 19 significant fluxes out of 24 in static versus laminar comparison (*Figure 5*). Two fluxes, isoleucine transaminase (*ILETA*) and 2-hydroxy-3-methylvalerate formation_c (*2H3MVc*),

showed a positive flux (flipped) was noted in the latter comparison (*Figure 5, panel (B)*). Furthermore, three additional significant fluxes were present – 2-oxoisovalerate dehydrogenase_m (*OIVID1m*), enoyl-CoA hydratase_m (*ECOAH12m*), and 3-hydroxyisobutyryl-CoA hydrolase_m (*3HBCOAHLm*).

The transamination reactions of BCAAs manifest in the fluxes of these AAs among different cellular compartments, but predominantly in the mitochondria (indicated by the suffix *_m*). This is demonstrated from the activities involving the transamination of leucine, valine, and isoleucine in the mitochondria, denoted by *LEUTAm*, *VALTAim*, and *ILETAm*, respectively. This is further substantiated by the downstream fluxes following the transamination of the BCAAs, specifically for *VALTAim* and *ILETAm*. To take *ILETAm* as an example, there are 6 intermediate fluxes that takes part in the metabolism of isoleucine and α-ketoglutarate all the way to produce building blocks for the acetyl-CoA pathway.

A possible driving force behind the differences in fluxes (both value and being present only in static versus laminar) could be attributed to the boundary modifications set for the exchange rate of NAD^+ as it was decreased for static conditions. Hence, fluxes the following downstream intermediate steps following transamination of valine *ECOAH12m* and *3HBCOAHLm* are present only in this comparison. Further down the catabolism of valine is the synthesis of the metabolite methylmalonic acid_m (*HC00900_m*) through the flux methylmalonate semialdehyde Oxidoreductase (*r0643*). In these final steps of valine catabolism, we observed substantial flux as to which valine gets degraded into methylmalonic acid_m and eventually into succinyl-CoA (classifying valine as a glucogenic AA). We hypothesize that the synthesis of succinyl-CoA, a key intermediate involved in the TCA cycle is to either produce more ATP to meet energy demands as it gets metabolized into pyruvate or serve as biosynthetic precursors that leads to heme-containing proteins to perform oxidative functions in response to oscillatory flow conditions in ECs. As for the degradation process of isoleucine, this glucogenic and ketogenic AA yields propionyl-CoA that gets converted into succinyl-CoA through biotin and vitamin B_{12}-requiring reactions or acetyl-CoA which can be used to replenish the anaplerotic supply of the TCA cycle intermediates.

3.4.3 Leukotrienes, prostaglandins, and thromboxane synthesis points to a possible inflamed state of endothelial cells in disturbed flow

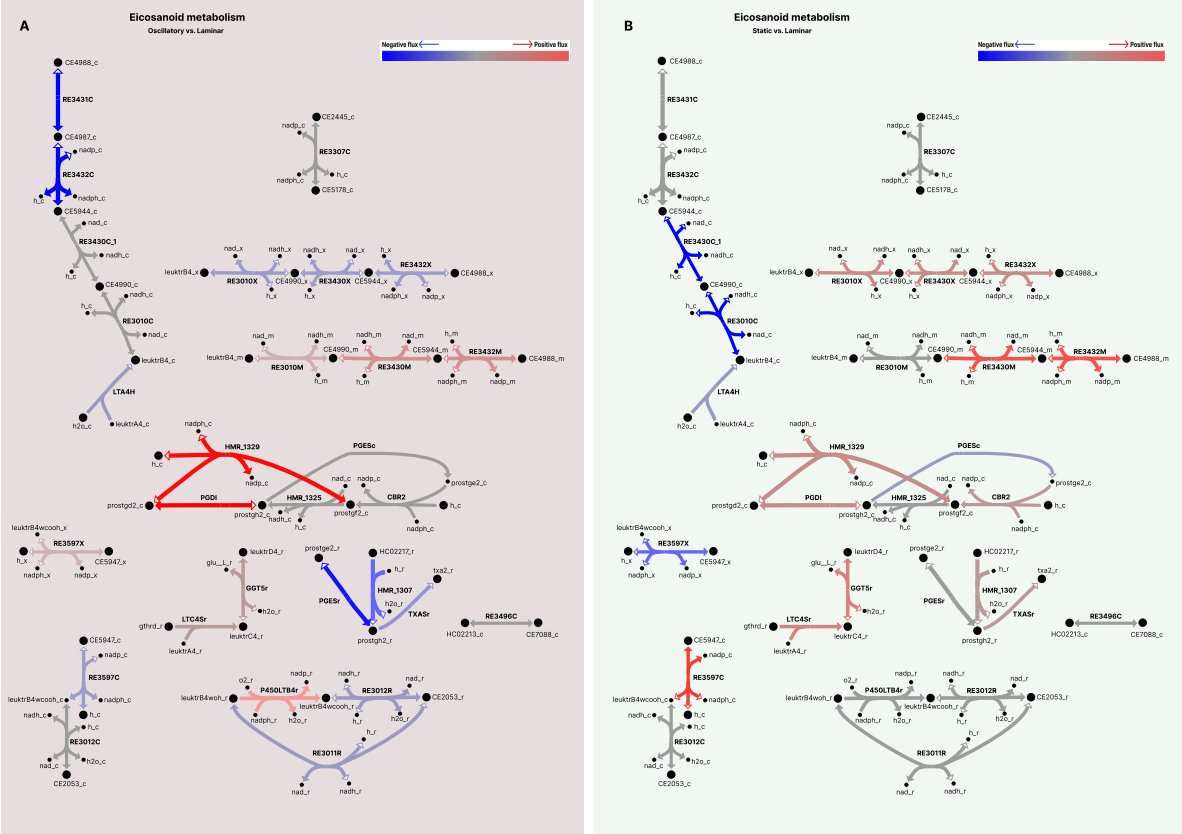

Figure 6 - Visualization of the enriched pathway for eicosanoid metabolism where panel (A) is Oscillatory vs. Laminar flow, and panel (B) is Static condition vs. Laminar flow. In panel (A), 22 out of 30 fluxes were identified as significant in the oscillatory vs. laminar comparison. In panel (B), the static vs. laminar comparison revealed 19 significant fluxes out of 24 (see Table 2 for the corrected p-value for both comparisons). The rest of the pathway maps follows the same pattern as Figure 4 in relation to the colours.

The eicosanoids (prostaglandins, leukotrienes, and thromboxanes) in ECs plays an important uniform role in many cardiovascular diseases (CVDs), the leading cause of global mortality and morbidity[136]. Eicosanoids are potent bioactive lipid derivatives, mainly derived from arachidonic acid through enzymatic pathways, mostly involving cyclooxygenases (COX) and lipoxygenases[136]. These lipids mediators that are being synthesized, such as the prostaglandins (PGE2, PGD2, and PGI2), leukotrienes (LTB4 and LTC4), and thromboxanes (TXA2) are essential for inflammation and vascular functions[137]. For example, PGI2 and TXA2 provoke antagonistic effects on muscular tone of the vessels and activation of platelets, acting fundamentally in the mechanism of flow regulation and mechanisms of coagulation[138]. Leukotrienes, such as LTB4, are stronger chemoattractants for leukocytes and increase vascular permeability, which may provide additional factors in the development of the local inflammatory milieu in the atherosclerotic lesion[136,137].

From the comparison of the results with the laminar flow condition, both oscillatory and static conditions gave a significant flux variation. Out of 30 fluxes, 22 were found significant in the comparison oscillatory versus laminar, and 19 in the comparison static versus laminar (*Figure 6*), as identified by eicosanoid metabolism PEA.

In the oscillatory versus laminar comparison, numerous fluxes responsible for the catalyzation of carbonyl reductase NADPH reactions leading to leukotrienes were identified. This is apparent through the fluxes at the bottom of (*Figure 6, panel (A)*), which involves cytochrome P450 LTB4_r (*P450LTB4r*), aldehyde dehydrogenase_r NAD^+ (*RE3012R*), and alcohol dehydrogenase_r (*RE3011R*). The LTC4 synthase_r (*LTC4Sr*), and gamma-glutamyltransferase 5_r (*GGT5r*), position at the top left of this trio of fluxes. This did not, however, quite reach significance in the latter comparison (*Figure 6, panel (B)*), where no significance was indeed seen in the trio-flux comparisons of *P450LTB4r*, *RE3012R*, and *RE3011R*. However, fluxes *LTC4Sr* and *GGT5r* were present.

Relative to the fluxes associated with the prostaglandins and thromboxanes, our PEA results indicated the same flux present in the analysis for each of the eicosanoids. For example, the second trios of fluxes were PGE synthase_r (*PGESr*), prostaglandin-endoperoxide synthase_r (*HMR_1307*), and TxA synthase_r (*TXASr*). In the oscillatory versus laminar analysis, a rather large flux is present in the synthesis of *PGH2* and then converted into *PGE2* and *TxA2*. However, for static versus laminar, two fluxes *HMR_1307* and *TXASr* are present only. Furthermore, the PEA highlights five other notable fluxes involved in the synthesis of prostaglandins: PGD2 11-reductase (*HMR_1329*), PGH2 D-isomerase (*PGDI*), *HMR_1325*, PGE synthase_c (*PGESc*), and carbonyl reductase NADPH (CBR2). In the oscillatory versus laminar comparison, substantial flux activity was observed through *HMR_1329* and *PGDI*, in contrast to the static versus laminar comparison. However, the remaining three fluxes did not show significant activity in the first comparison, with only *PGESc* and *CBR2* being significant in the latter comparison.

Our PEA results from both comparisons indicate a clear trend of fluxes toward the synthesis of leukotrienes, such as LTD4, and more prominently, LTB4 and its derivatives. Moreover, these compounds are synthesized in different cellular compartments. For *LTD4_r*, synthesis occurs through the fluxes *LTC4Sr* and *GGT5r*, which first involve the conversion of reduced glutathione_r (*gthd_r*) to *LTA4_r*, and subsequently, the gamma-glutamyltransferase reaction catalyzes the formation of *LTD4_r.* Regarding LTB4 derivatives, multiple fluxes contribute to the synthesis of these molecules. Specifically, the fluxes *RE3010X*, *RE3430X*, and *RE3432X* facilitate the conversion of *LTB4_x* through a series of 5-lipoxygenase reactions to initially produce 12-oxo-LTB4_x (*CE4990_x*), a less active form of LTB4. Subsequently, *CE4990_x* undergoes further reduction and oxidation modifications (introducing a ketone group) at the 12^{th} carbon position to form 10,11-dihydro-12-oxo-LTB4_x (*CE5944_x*). Finally, 10,11-dihydro-12-epi-LTB4_x (*CE4988_x*) is produced, where an epimerization change occurs at the 12^{th} position. Additionally, our results reveal the presence of these fluxes in both the mitochondria and cytosol, as evidenced by mitochondrial fluxes *RE3010M* (observed exclusively in oscillatory versus laminar conditions), *RE3430M*, and *RE3432M*, and cytosolic fluxes *RE3432C*, *RE3431C*, *LT4AH*, *RE3010C*, and *RE3430C_1* (Note: that *RE3432C* and *RE3431C* were significant only in oscillatory versus laminar conditions (*Figure 6, panel (A)*), while *LT4AH*, *RE3010C*, and *RE3430C_1* were only prominent in static versus laminar comparison (*Figure 6, panel (B)*). These LTB4 derivatives are synthesized across almost all tissues and act locally. We assume that the effect of the disturbed flow (oscillatory) or absence of flow, ECs funnel their fluxes to synthesize leukotrines as a way to mediate inflammation.

As for prostaglandin and thromboxane synthesis, we see fluxes (*PGESr, HMR_1307, TXAS4, PGDI, HMR_1329, PGESc, CBR2*, and *HMR_1325*) feeding into the synthesis of PGH2 which yields different types of prostaglandins and thromboxanes. The conversion of these derivatives is then dictated by cell-specific synthases such as COX-1 and COX-2. Presence of these fluxes towards synthesizing these compounds imply that in the context of oscillatory versus laminar, the ECs are experiencing more inflammation due to a greater number of prostaglandins and thromboxanes being produced in comparison to static versus laminar. Also, we see a strong disposition to synthesizing PGE2 and PGF2 which in ECs, plays a key role in vasoconstriction and vasodilation perhaps in response to when flow is slowed (oscillatory) or blocked (static). Lastly, synthesis of TXA2 which promotes platelet adhesion, aggregation, and vascular smooth muscle contractions and therefore, causes thrombi may further hint at the distressed conditions ECs due to oscillatory flow and static condition.

3.5 Static specific metabolic flux perturbations.

3.5.1 Fluxes in the arachidonic acid metabolism show characteristics of synthesizing pro- and anti-inflammatory lipid mediators

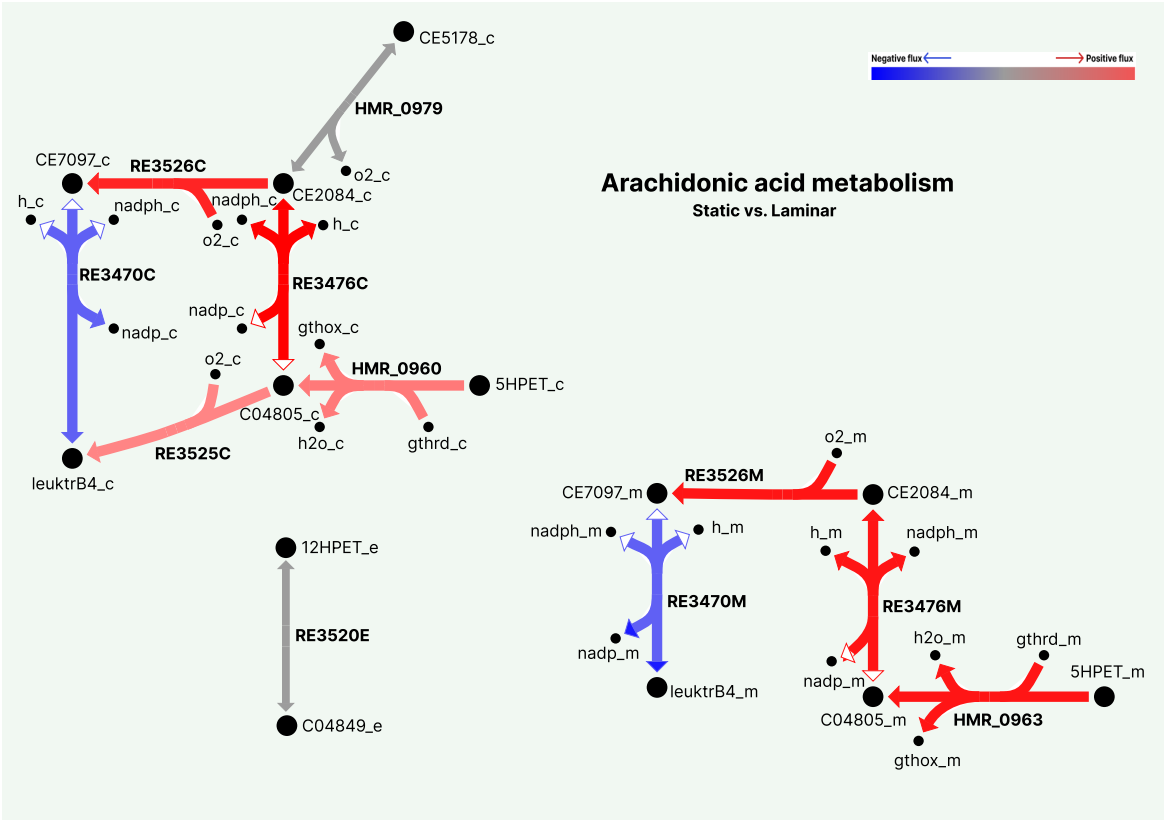

Figure 7 – Visualization of the enriched pathway arachidonic acid metabolism. This figure illustrates the arachidonic acid metabolism pathway, significant only in the comparison between static condition vs. laminar flow. Out of the 12 fluxes analyzed, 10 were found significant (see Table 2 for the corrected p-value). The rest of the pathway maps follows the same pattern as Figure 4 in relation to the colours.

Arachidonic acid metabolism is carried out via several critical enzymatic pathways: 5- and 12-lipoxygenases oxygenates arachidonic acid to produce 5-hydropeoxyeicosatetronoic acid (5-HPETE) and 12-hydroperoxyeicosatetraenoic acid (12-HPETE), respectively[139]. These metabolites exhibit significant biochemical activity in the cell, which influences the modulation of diverse cellular processes that are mainly related to signal transduction and membrane dynamics. LTB4, a derivative of arachidonic acid, is synthesized through the lipoxygenase pathway and acts as a potent mediator, binding to specific receptors of endothelial cells, thus having an influence on various cellular functions[136,140].

The PEA results for arachidonic acid metabolism reveal two distinct reaction complexes characterized by mitochondrial or cytosolic compartmentalization (*Figure 7*). Our analysis identified 10 significant fluxes out of 12 observed. In the mitochondrial compartment, notable fluxes include glutathione peroxidase (*HMR_0963*), carbonyl reductase_m NADPH (*RE3476M*), arachidonate 12-lipoxygenase_m (*RE3526M*), and another instance of carbonyl reductase_m NADPH (*RE3470M*). These fluxes predominantly contribute to the production of 5-HPETE_m (*CE7097_m*). A similar pattern is observed in the cytosol, where all significant fluxes are directed towards the synthesis of 5-HPETE_c (*CE7097_c*), reflecting a coordinated metabolic response across cellular compartments.

Fluxes within this pathway are characterized by the synthesis of 5-oxo-12(S)-hydroxy-eicosa-6E,8Z,10E,14Z-tetraenoate (*CE7097_m* and *CE7097_c*), catalyzed by the arachidonate 12-lipoxygenase reaction in both the mitochondria and cytosol. The observed pattern of fluxes driving the synthesis of *CE7097* suggests a dysfunctional state in ECs under static conditions. This inference is drawn from the products of *CE7097* having multiple effects on the overall EC integrity such as inducing inflammation, increasing vascular permeability and other vascular disease.

3.5.2 Multiple pathways converge in the TCA cycle

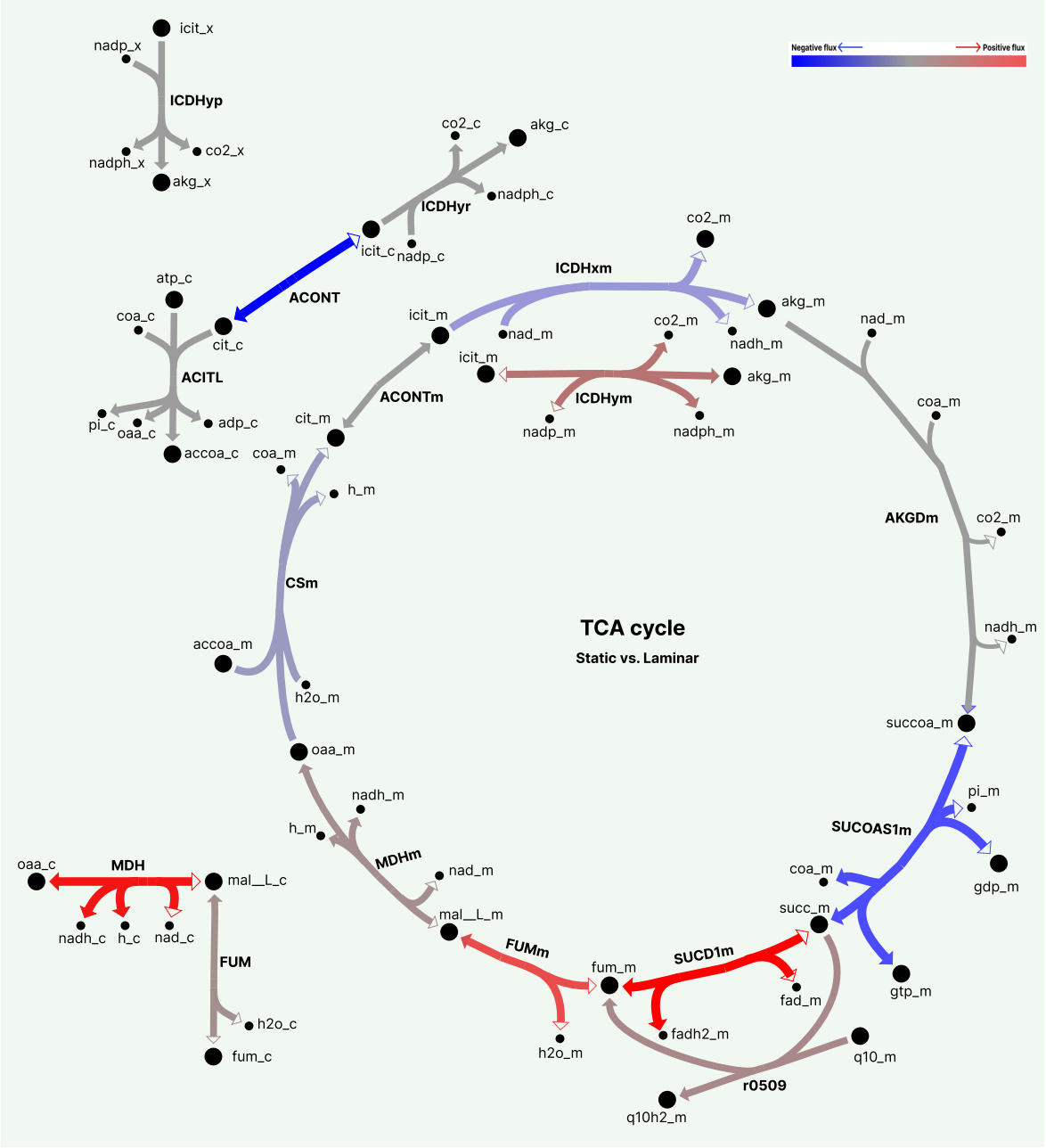

Figure 8 – Visualization of TCA cycle. Our PEA reveals that the TCA cycle was also found to be significant solely in the comparison between the static condition and laminar flow. Among the 16 fluxes evaluated, 11 were identified as significant (see Table 2 for the corrected p-value. The rest of the pathway maps follows the same pattern as Figure 4 in relation to the colours.

Our analysis identifies the TCA cycle as a notably enriched pathway in the comparison between static condition and laminar flow. In this PEA, 11 significant fluxes out of 16 were identified (*Figure 8*). The core of the TCA cycle comprises eight essential fluxes; however, only six were observed in our analysis. These include isocitrate dehydrogenase_m (*ICDHxm* or *ICDHym*), 2-oxoglutarate dehydrogenase_m (*AKGDm*), succinate-CoA ligase_m (*SUCOAS1m*), succinate dehydrogenase_m (*SUCD1m*), fumarase_m (*FUMm*), malate

dehydrogenase_m (*MDHm*), citrate synthase_m (*CSm*) and aconitase_m (ACONTm). Additionally, other notable fluxes were observed in the cytosol, specifically involving *MDH*, *FUM*, and *ACONT*. Majority of the aforementioned pathways in our results either converges in the TCA cycle or they are largely involved with the anabolism or catabolism of the intermediates synthesized in this pathway.

The TCA cycle starts with the irreversible condensation of acetyl-CoA and OAA to form citrate via the flux *CSm*. It is noteworthy to mention that the point of origin of acetyl-CoA is not within the TCA cycle and, in fact, can be synthesized through several metabolic pathways. Primarily, acetyl-CoA is derived from glycolysis under the mediation of the pyruvate dehydrogenase complex. However, there are alternate sources such as AAs, including BCAAs and FAO in ECs. As described in Section 3.3.2, isoleucine (leucine as well, but fluxes involved in further catabolism were found to be not significant) classifies as both glucogenic and ketogenic which perhaps be one of the sources for acetyl-CoA in TCA cycle.

Subsequent to citrate synthesis, citrate is then isomerized through the aconitase flux *ACONTm* (not significant in our PEA) to produce isocitrate. Thereafter, isocitrate undergoes another irreversible reaction called oxidative decarboxylation through fluxes *ICDHxm* or *ICDHym*. This is a rate-limiting step in the TCA cycle, yielding α-ketoglutarate along with the release of the first molecule of CO_2. Our analysis showed distinctly that there are two isocitrate dehydrogenase fluxes that differ in their cofactor preference: *ICDHxm* uses NAD^+ to form NADH and *ICDHym* uses $NADP^+$ to give NADPH. The presence of *ICDHym* suggests that it may be involved in anabolic reactions, such as FAO, lipid synthesis, and maintenance of glutathione levels in ECs.

The third and final irreversible oxidation decarboxylation reaction converts α-ketoglutarate to succinyl-CoA through the flux *AKDGm* (not significant in our PEA). Succinyl-CoA is subsequently cleaved by the flux *SUCOAS1m*, yielding succinate. Our findings showed high flux through SUCOAS1m which favours the conversion of succinate to succinyl-CoA and formation of GDP from GTP. We postulate, therefore, that the TCA cycle can also receive succinyl-CoA from alternative sources, such as that from isoleucine catabolism, which yields propionyl-CoA, subsequently converted into succinyl-CoA. After succinate formation, oxidation mediated by the flux *SUCD1m* yields fumarate. Another possible route to produce fumate is through an additional flux through succinate ubiquinone reductase_m (r0509), which, in addition to fumarate, catalyzes the conversion of ubiquinone to ubiquinol. Then, fumarate is further hydrated by the flux *FUM*_m to form malate. In addition to these, reactions for the TCA to provide the cell with NADH and OAA through the last flux in this cycle *MDHm*.

4 Discussion

In this work, we generated three context-specific GEMs of ECs that were subjected to laminar, static, and oscillatory conditions using the rFASTCORMICS algorithm[98]. Not only that, but these models were further constrained using our metabolomics data consisting of 56 uptake and secretion rates of metabolites. These representative context-specific and constrained GEMs allowed us to predict the metabolic flux perturbations that occurs in disturbed flow and static conditions. To this end, our results are consistent with previous literatures that covers the effect of different flow regimes in context to the significantly altered pathways we observed. rFASTCORMICS, primarily intended for cancer research, have been instrumental in building high-quality GEMs using RNA-Seq data from colorectal cancer. The authors of rFASTCORMICS showed that thousands of model reconstructions enabled the finding of potential drug targets and the repurposing of existing drugs that showed significant effect in decreasing cancer cell proliferation[98]. Furthermore, rFASTCORMICS has also been applied and has produced profound insights in melanoma cancer research. Reconstructed metabolic models identified metabolic dependencies that are distinct to melanoma cells and differ significantly from normal cells in patient data. All these models are pinpointing the potential targets of therapeutic approaches and possible opportunities for drug repurposing that will have effective activity on the key metabolic pathways driving progression in melanomas[99]. Considering the success of rFASTCORMICS in cancer research, specifically in drug target prediction of drug repurposing. This avenue maybe a promising route to further expand this work to potentially identify novel drug targets or drug repurposing strategies for vascular-related diseases.

The modulation of lipid metabolism in ECs, especially under varying flow conditions suggests a dynamic adjustment to inflammatory states present in many cardiovascular CVDs. These efforts are likely aimed at mediating pathophysiological processes or in response to mechanical stresses (due to blood flow) to maintain healthy vascular health. The observed changes in eicosanoid metabolism as seen in the results PEA (*Figure 6*) and arachidonic acid metabolism (*Figure 7*), particularly the increased synthesis of eicosanoids (prostaglandins, leukotrienes and thromboxanes) as well as fluxes being channeled to catalyze arachidonate 12-lipoxygenase reactions are phenotypical traits that have been characterized in inflammation[136,138,141,142]. These findings are in line with studies that have shown the metabolomic profiles during the pathogenesis of CAVD such as calcified aortic valve stenosis (CAVS), aortic stenosis (AS), and coronary artery diseases (CAD)[143–145]. In a study where untargeted analysis was used to profile the pathomechanism of CAVS, the significance of significantly altered pathways was explicitly noted[145]. Using clinically relevant hemodynamic estimates such mean pressure gradient (MPG), aortic valve area (AVA), and AV calcification score, they established arachidonic acid, linoleic acid, and glycerophospholipids to be associated. Additionally, in a study done pertaining AS and CAD patients, synthesis of eicosanoids was found to be increased in both cases which is also reflected in our PEA results[143,144].

In cancer research, the TCA cycle and its intermediates have been associated in playing a pivotal role not only as an energy source but also in supporting the high biosynthetic needs in fast proliferating tumor cells[146]. Several studies have demonstrated remarkable metabolic flexibility in cancer cells, particularly from glioblastomas and metastatic brain tumors[147,148]. For example, although most tumors depend on glucose for energy, some are able to oxidize alternative substrates such as acetate, especially in conditions where normal energy sources are not available or are in limited quantities[147]. Moreover, acetate has been implicated in its

reliance to acetyl-CoA synthetase enzyme 2 (ACSS2) to introduce a large portion of carbon into the acetyl-CoA supply that is crucial in the synthesis of FAs and phospholipids.[148,149] This characteristic metabolic adaptation of cancer is crucial for the survival and growth of the tumor in such a metabolically stressed condition, due to hypoxia or nutrient deprivation[148]. Additionally, other research have underline the complexity of cancer metabolism, where TCA cycle intermediates such as citrate, derived from glucose and acetate, serve a dual role in energy production and biosynthesis[150]. For this reason, intermediates of the TCA cycle have roles that extends beyond metabolism and shape into signaling molecules that influences tumor behaviour. Another example is a study where accumulation of succinate due to a mutation in SDH can lead to enhanced stabilization of hypoxia-inducible factor (HIFs) in a tumor under normoxic conditions[150]. This suggests that the higher the stabilization of HIFs, the higher the vascularization and survival of the same conditions, showing a very clear link between TCA cycle dysfunction and oncogenic signaling. A distinct metabolic route involving glutamine's conversion into α-ketoglutarate is crucial for understanding how cancer cells utilize glutamine to fulfil their biosynthetic demands for growth and proliferation. This specific flux proclivity in synthesizing α-ketoglutarate was observed in the PEA of glutamate metabolism (*Figure 4*) for both comparisons. After synthesis, α-ketoglutarate can enter the TCA cycle and serve as an anaplerotic replenishment or undergo reductive decarboxylation forming isocitrate which can take part in FAO activities *(Figure 8*). The characteristic trend of reductive carboxylation has been implicated in various cancer studies and emphasized for its importance in the metabolic adaptations during tumor progressions[151–153]. Previous literature has suggested that α-ketoglutarate plays a key role in regulating HIFs as it can act as substrate for prolyl hydroxylase[154]. This regulation links cellular metabolism to the transcriptional control of genes responsible for angiogenesis and survival in the hypoxic environment of tumor. Therefore, the importance of how glutamine metabolism is utilized in cancer metabolism has led to potential therapeutic targets such as glutaminase inhibitors[151,155].

Glaring limitations of this work can be extended in computational modelling aspects. In the initial stages of the project, several context-specific algorithms were considered such as GIMME and iMAT[101,102]. However, in reviewing the methodologies of GIMME and iMAT as well as reading journal reviews of these algorithms (and others). We decided to move forward with rFASTCORMICS based on several reasons [98]. First, GIMME was tailored to use RNA-Seq data from skeletal muscle cells and *E.coli*. Not only that, GIMME required a specific threshold to be defined to classify high/low gene expression state which we posed as a limitation, and an a priori knowledge of the objective function to be maximized. Secondly, the iMAT algorithm, though this algorithm did not require a metabolic objective to be maximized, the predicted metabolic fluxes would be too broad due the algorithms implementation in discretizing gene expression data into tri-value expression states[96,156]. However, there is great value in assesing whether our findings in using rFASTCORMICS would be in line with other algorithms as a quality check of models generated. In addition to model reconstructions, we perhaps might have benefited from using a more annotated human metabolic model HUMAN1 instead of Recon 3D[88,89]. Integrating HUMAN1 may have offered more reactions during our anaylsis which in turn could have offer us better insights to the complexities of EC metabolism.

The future work of this project would be the experimental validations of our findings. This would greatly deepen not only our understanding of the EC metabolism but also, attest to the predictive capabilities of metabolic models. In addition to the limitations posed in our chosen reconstruction methods (rFASTCORMICS and Recon 3D), insights using single-cell RNA-Seq dataset would have maybe offered us a much more fine-grained understanding in

the metabolic perturbations of different flow regimes. The adoption of a single-cell dataset would allow the exploration the single-cell version of rFASTCORMICS called scFASTCORMICS[157]. Lastly, a potential project that could stem from the outputs of this project would be to use our reconstructed metabolic models as "base-models" and infer the behaviour of metabolic pertubations in ECs from other diseased datasets.

5 Conclusions

In conclusion, this present work further elucidates the biological implications on EC metabolism under varying flow regimes using GEMs developed with the rFASTCORMICS algorithm. Through integration of transcriptomics and metabolomics data, our findings reveal significant metabolic pathway perturbations in the TCA cycle, glutamate, BCAAs, as well as eicosanoid and arachidonic acid metabolism under oscillatory, laminar, and static conditions. These perturbations allude to the metabolic adaptation of ECs in response to mechanical forces. Lastly, our data strongly emphasize the complex interplay of mechanical cues and metabolic behavior in which targeting of key metabolic pathways might be a critical determinant for the maintenance of vascular health and for prevention of flow-related vascular diseases.

References

1. King, J. & Lowery, D. R. *Physiology, Cardiac Output*. (2024).

2. Fang, Y., Wu, D. & Birukov, K. G. Mechanosensing and Mechanoregulation of Endothelial Cell Functions. *Compr Physiol* **9**, 873–904 (2019).

3. Krüger-Genge, A., Blocki, A., Franke, R.-P. & Jung, F. Vascular Endothelial Cell Biology: An Update. *Int J Mol Sci* **20**, (2019).

4. Li, J. *et al.* Mechanosensitive super-enhancers regulate genes linked to atherosclerosis in endothelial cells. *J Cell Biol* **223**, (2024).

5. Hahn, C. & Schwartz, M. A. Mechanotransduction in vascular physiology and atherogenesis. *Nat Rev Mol Cell Biol* **10**, 53–62 (2009).

6. Davies, P. F., Civelek, M., Fang, Y. & Fleming, I. The atherosusceptible endothelium: endothelial phenotypes in complex haemodynamic shear stress regions in vivo. *Cardiovasc Res* **99**, 315–327 (2013).

7. Vink, H., Constantinescu, A. A. & Spaan, J. A. E. Oxidized Lipoproteins Degrade the Endothelial Surface Layer. *Circulation* **101**, 1500–1502 (2000).

8. Van der Heiden, K. *et al.* Endothelial primary cilia in areas of disturbed flow are at the base of atherosclerosis. *Atherosclerosis* **196**, 542–550 (2008).

9. Henderson-Toth, C. E., Jahnsen, E. D., Jamarani, R. & Al-Roubaie, S. The glycocalyx is present as soon as blood flow is initiated and is required for normal vascular development. *Dev Biol* **369**, 330–339 (2012).

10. Ebong, E. E., Lopez-Quintero, S. V, Rizzo, V., Spray, D. C. & Tarbell, J. M. Shear-induced endothelial NOS activation and remodeling via heparan sulfate, glypican-1, and syndecan-1. *Integr. Biol.* **6**, 338–347 (2014).

11. Dinsmore, C. J. & Reiter, J. F. Endothelial primary cilia inhibit atherosclerosis. *EMBO Rep* **17**, 156–166 (2016).

12. Pahakis, M. Y., Kosky, J. R., Dull, R. O. & Tarbell, J. M. The role of endothelial glycocalyx components in mechanotransduction of fluid shear stress. *Biochem Biophys Res Commun* **355**, 228–233 (2007).

13. Zeng, Y. Endothelial glycocalyx as a critical signalling platform integrating the extracellular haemodynamic forces and chemical signalling. *J Cell Mol Med* **21**, 1457–1462 (2017).

14. Reitsma, S., Slaaf, D. W., Vink, H., van Zandvoort, M. A. M. J. & oude Egbrink, M. G. A. The endothelial glycocalyx: composition, functions, and visualization. *Pflugers Arch* **454**, 345–359 (2007).

15. Mochizuki, S. *et al.* Role of hyaluronic acid glycosaminoglycans in shear-induced endothelium-derived nitric oxide release. *Am J Physiol Heart Circ Physiol* **285**, H722-726 (2003).

16. Voyvodic, P. L. *et al.* Loss of Syndecan-1 Induces a Pro-inflammatory Phenotype in Endothelial Cells with a Dysregulated Response to Atheroprotective Flow. *Journal of Biological Chemistry* **289**, 9547–9559 (2014).

17. Hierck, B. P. *et al.* Primary cilia sensitize endothelial cells for fluid shear stress. *Developmental Dynamics* **237**, 725–735 (2008).

18. M. Mohieldin, A. *et al.* Vascular Endothelial Primary Cilia: Mechanosensation and Hypertension. *Curr Hypertens Rev* **12**, 57–67 (2016).

19. Nauli, S. M. *et al.* Endothelial Cilia Are Fluid Shear Sensors That Regulate Calcium Signaling and Nitric Oxide Production Through Polycystin-1. *Circulation* **117**, 1161–1171 (2008).

20. AbouAlaiwi, W. A. *et al.* Ciliary Polycystin-2 Is a Mechanosensitive Calcium Channel Involved in Nitric Oxide Signaling Cascades. *Circ Res* **104**, 860–869 (2009).

21. Gupta, A. *et al.* Cilia proteins are biomarkers of altered flow in the vasculature. *JCI Insight* **7**, (2022).

22. Goetz, J. G. *et al.* Endothelial Cilia Mediate Low Flow Sensing during Zebrafish Vascular Development. *Cell Rep* **6**, 799–808 (2014).

23. Gopalakrishnan, J. *et al.* Emerging principles of primary cilia dynamics in controlling tissue organization and function. *EMBO J* **42**, (2023).

24. Pala, R., Jamal, M., Alshammari, Q. & Nauli, S. M. The Roles of Primary Cilia in Cardiovascular Diseases. *Cells* **7**, (2018).

25. Luu, V. Z., Chowdhury, B., Al-Omran, M., Hess, D. A. & Verma, S. Role of endothelial primary cilia as fluid mechanosensors on vascular health. *Atherosclerosis* **275**, 196–204 (2018).

26. Pi, X., Xie, L. & Patterson, C. Emerging roles of vascular endothelium in metabolic homeostasis. *Circ Res* **123**, 477–494 (2018).

27. Eelen, G. *et al.* Endothelial Cell Metabolism. *Physiol Rev* **98**, 3–58 (2018).

28. Li, X., Sun, X. & Carmeliet, P. Hallmarks of Endothelial Cell Metabolism in Health and Disease. *Cell Metab* **30**, 414–433 (2019).

29. D'Alessio, A. Role of Endothelial Cell Metabolism in Normal and Tumor Vasculature. *Cancers (Basel)* **15**, 1921 (2023).

30. Eelen, G., de Zeeuw, P., Simons, M. & Carmeliet, P. Endothelial Cell Metabolism in Normal and Diseased Vasculature. *Circ Res* **116**, 1231–1244 (2015).

31. Dejana, E., Hirschi, K. K. & Simons, M. The molecular basis of endothelial cell plasticity. *Nat Commun* **8**, (2017).

32. Harraz, O. F. Endothelial cell metabolism and vascular function: A paradigm shift? *Function* **4**, (2023).

33. Ricard, N., Bailly, S., Guignabert, C. & Simons, M. The quiescent endothelium: signalling pathways regulating organ-specific endothelial normalcy. *Nat Rev Cardiol* **18**, 565–580 (2021).

34. Wilson, C., Lee, M. D., Buckley, C., Zhang, X. & McCarron, J. G. Mitochondrial ATP production is required for endothelial cell control of vascular tone. *Function* **4**, (2022).

35. Krützfeldt, A. Metabolism of exogenous substrates by coronary endothelial cells in culture. *J Mol Cell Cardiol* **22**, 1393–1404 (1990).

36. Groschner, L. N., Waldeck-Weiermair, M., Malli, R. & Graier, W. F. Endothelial mitochondria—less respiration, more integration. *Pflugers Arch* **464**, 63–76 (2012).

37. Mertens, S., Noll, T., Spahr, R., Krutzfeldt, A. & Piper, H. M. Energetic response of coronary endothelial cells to hypoxia. *American Journal of Physiology-Heart and Circulatory Physiology* **258**, H689–H694 (1990).

38. Leung, S. W. S. & Shi, Y. The glycolytic process in endothelial cells and its implications. *Acta Pharmacol Sin* **43**, 251–259 (2022).

39. Davidson, S. M. & Duchen, M. R. Endothelial Mitochondria. *Circ Res* **100**, 1128–1141 (2007).

40. Becker, L. New concepts in reactive oxygen species and cardiovascular reperfusion physiology. *Cardiovasc Res* **61**, 461–470 (2004).

41. Koziel, A. & Jarmuszkiewicz, W. Hypoxia and aerobic metabolism adaptations of human endothelial cells. *Pflugers Arch* **469**, 815–827 (2017).

42. Culic, O., Decking, U. K. M. & Schrader, J. Metabolic adaptation of endothelial cells to substrate deprivation. *American Journal of Physiology-Cell Physiology* **276**, C1061–C1068 (1999).

43. Pircher, A., Treps, L., Bodrug, N. & Carmeliet, P. Endothelial cell metabolism: A novel player in atherosclerosis? Basic principles and therapeutic opportunities. *Atherosclerosis* **253**, 247–257 (2016).

44. Wang, G. *et al.* Shear Stress Regulation of Endothelial Glycocalyx Structure Is Determined by Glucobiosynthesis. *Arterioscler Thromb Vasc Biol* **40**, 350–364 (2020).

45. Basehore, S. E., Garcia, J. & Clyne, A. M. Steady Laminar Flow Decreases Endothelial Glycolytic Flux While Enhancing Proteoglycan Synthesis and Antioxidant Pathways. *Int J Mol Sci* **25**, 2485 (2024).

46. Zhenyukh, O. *et al.* Branched-chain amino acids promote endothelial dysfunction through increased reactive oxygen species generation and inflammation. *J Cell Mol Med* **22**, 4948–4962 (2018).

47. Zhenyukh, O. *et al.* High concentration of branched-chain amino acids promotes oxidative stress, inflammation and migration of human peripheral blood mononuclear cells via mTORC1 activation. *Free Radic Biol Med* **104**, 165–177 (2017).

48. Fernstrom, J. D. Branched-Chain Amino Acids and Brain Function. *J Nutr* **135**, 1539S-1546S (2005).

49. Jang, C. *et al.* A branched-chain amino acid metabolite drives vascular fatty acid transport and causes insulin resistance. *Nat Med* **22**, 421–426 (2016).

50. Yu, D. *et al.* The adverse metabolic effects of branched-chain amino acids are mediated by isoleucine and valine. *Cell Metab* **33**, 905-922.e6 (2021).

51. Newsholme, P., Procopio, J., Lima, M. M. R., Pithon-Curi, T. C. & Curi, R. Glutamine and glutamate?their central role in cell metabolism and function. *Cell Biochem Funct* **21**, 1–9 (2003).

52. Durante, W. The Emerging Role of l-Glutamine in Cardiovascular Health and Disease. *Nutrients* **11**, 2092 (2019).

53. Eelen, G. *et al.* Role of glutamine synthetase in angiogenesis beyond glutamine synthesis. *Nature* **561**, 63–69 (2018).

54. Kim, B., Li, J., Jang, C. & Arany, Z. Glutamine fuels proliferation but not migration of endothelial cells. *EMBO J* **36**, 2321–2333 (2017).

55. Cory, J. G. & Cory, A. H. Critical roles of glutamine as nitrogen donors in purine and pyrimidine nucleotide synthesis: asparaginase treatment in childhood acute lymphoblastic leukemia. *In Vivo* **20**, 587–589 (2006).

56. Savitz, J. The kynurenine pathway: a finger in every pie. *Mol Psychiatry* **25**, 131–147 (2020).

57. Wu, K. K., Kuo, C.-C., Yet, S.-F., Lee, C.-M. & Liou, J.-Y. 5-methoxytryptophan: an arsenal against vascular injury and inflammation. *J Biomed Sci* **27**, 79 (2020).

58. Ala, M. & Eftekhar, S. P. The Footprint of Kynurenine Pathway in Cardiovascular Diseases. *International Journal of Tryptophan Research* **15**, 117864692210966 (2022).

59. Baumgartner, R., Forteza, M. J. & Ketelhuth, D. F. J. The interplay between cytokines and the Kynurenine pathway in inflammation and atherosclerosis. *Cytokine* **122**, 154148 (2019).

60. Chu, L.-Y., Wang, Y.-F., Cheng, H.-H., Kuo, C.-C. & Wu, K. K. Endothelium-Derived 5-Methoxytryptophan Protects Endothelial Barrier Function by Blocking p38 MAPK Activation. *PLoS One* **11**, e0152166 (2016).

61. Song, P., Ramprasath, T., Wang, H. & Zou, M.-H. Abnormal kynurenine pathway of tryptophan catabolism in cardiovascular diseases. *Cellular and Molecular Life Sciences* **74**, 2899–2916 (2017).

62. Baumgartner, R. *et al.* Evidence that a deviation in the kynurenine pathway aggravates atherosclerotic disease in humans. *J Intern Med* **289**, 53–68 (2021).

63. Wang, Y.-F. *et al.* Endothelium-Derived 5-Methoxytryptophan Is a Circulating Anti-Inflammatory Molecule That Blocks Systemic Inflammation. *Circ Res* **119**, 222–236 (2016).

64. Ho, Y.-C. *et al.* A Novel Protective Function of 5-Methoxytryptophan in Vascular Injury. *Sci Rep* **6**, 25374 (2016).

65. Schoors, S. *et al.* Fatty acid carbon is essential for dNTP synthesis in endothelial cells. *Nature* **520**, 192–197 (2015).

66. De Bock, K., Georgiadou, M. & Carmeliet, P. Role of Endothelial Cell Metabolism in Vessel Sprouting. *Cell Metab* **18**, 634–647 (2013).

67. Kalucka, J. *et al.* Quiescent Endothelial Cells Upregulate Fatty Acid β-Oxidation for Vasculoprotection via Redox Homeostasis. *Cell Metab* **28**, 881-894.e13 (2018).

68. Patella, F. *et al.* Proteomics-Based Metabolic Modeling Reveals That Fatty Acid Oxidation (FAO) Controls Endothelial Cell (EC) Permeability. *Molecular & Cellular Proteomics* **14**, 621–634 (2015).

69. Pokharel, M. D. *et al.* Metabolic reprogramming, oxidative stress, and pulmonary hypertension. *Redox Biol* **64**, 102797 (2023).

70. Fessel, J. P. *et al.* Metabolomic Analysis of Bone Morphogenetic Protein Receptor Type 2 Mutations in Human Pulmonary Endothelium Reveals Widespread Metabolic Reprogramming. *Pulm Circ* **2**, 201–213 (2012).

71. Yan, S., Zhang, J., Zhang, T., Li, Y. & Li, X. Advances in endothelial cell lipid metabolism and tumor angiogenesis. *Results Chem* **7**, 101467 (2024).

72. De Bock, K., Georgiadou, M. & Carmeliet, P. Role of Endothelial Cell Metabolism in Vessel Sprouting. *Cell Metab* **18**, 634–647 (2013).

73. Xiong, Y. & Hla, T. S1P Control of Endothelial Integrity. in 85–105 (2014). doi:10.1007/978-3-319-05879-5_4.

74. Lee, H., Goetzl, E. J. & An, S. Lysophosphatidic acid and sphingosine 1-phosphate stimulate endothelial cell wound healing. *American Journal of Physiology-Cell Physiology* **278**, C612–C618 (2000).

75. Schaphorst, K. L. *et al.* Role of sphingosine-1 phosphate in the enhancement of endothelial barrier integrity by platelet-released products. *American Journal of Physiology-Lung Cellular and Molecular Physiology* **285**, L258–L267 (2003).

76. Akbari, E. *et al.* Endothelial barrier function is co-regulated at vessel bifurcations by fluid forces and sphingosine-1-phosphate. *Biomaterials and Biosystems* **3**, 100020 (2021).

77. Nauli, S. M. *et al.* Endothelial Cilia Are Fluid Shear Sensors That Regulate Calcium Signaling and Nitric Oxide Production Through Polycystin-1. *Circulation* **117**, 1161–1171 (2008).

78. Kuhlencordt, P. J. *et al.* Role of endothelial nitric oxide synthase in endothelial activation: insights from eNOS knockout endothelial cells. *American Journal of Physiology-Cell Physiology* **286**, C1195–C1202 (2004).

79. Janaszak-Jasiecka, A., Siekierzycka, A., Płoska, A., Dobrucki, I. T. & Kalinowski, L. Endothelial Dysfunction Driven by Hypoxia—The Influence of Oxygen Deficiency on NO Bioavailability. *Biomolecules* **11**, 982 (2021).

80. Tran, N. *et al.* Endothelial Nitric Oxide Synthase (eNOS) and the Cardiovascular System: in Physiology and in Disease States. *Am J Biomed Sci Res* **15**, 153–177 (2022).

81. Zhang, C. & Hua, Q. Applications of Genome-Scale Metabolic Models in Biotechnology and Systems Medicine. *Front Physiol* **6**, (2016).

82. Kim, B., Kim, W. J., Kim, D. I. & Lee, S. Y. Applications of genome-scale metabolic network model in metabolic engineering. *J Ind Microbiol Biotechnol* **42**, 339–348 (2015).

83. Thiele, I. & Palsson, B. Ø. A protocol for generating a high-quality genome-scale metabolic reconstruction. *Nat Protoc* **5**, 93–121 (2010).

84. Masid, M. & Hatzimanikatis, V. Quantitative modeling of human metabolism: A call for a community effort. *Curr Opin Syst Biol* **26**, 109–115 (2021).

85. Aurich, M. K. *et al.* Prediction of intracellular metabolic states from extracellular metabolomic data. *Metabolomics* **11**, 603–619 (2015).

86. Bernstein, D. B., Sulheim, S., Almaas, E. & Segrè, D. Addressing uncertainty in genome-scale metabolic model reconstruction and analysis. *Genome Biol* **22**, 64 (2021).

87. King, Z. A. *et al.* BiGG Models: A platform for integrating, standardizing and sharing genome-scale models. *Nucleic Acids Res* **44**, D515–D522 (2016).

88. Robinson, J. L. *et al.* An atlas of human metabolism. *Sci Signal* **13**, (2020).

89. Brunk, E. *et al.* Recon3D enables a three-dimensional view of gene variation in human metabolism. *Nat Biotechnol* **36**, 272–281 (2018).

90. Blais, E. M. *et al.* Reconciled rat and human metabolic networks for comparative toxicogenomics and biomarker predictions. *Nat Commun* **8**, 14250 (2017).

91. Mardinoglu, A. *et al.* Genome-scale metabolic modelling of hepatocytes reveals serine deficiency in patients with non-alcoholic fatty liver disease. *Nat Commun* **5**, 3083 (2014).

92. King, Z. A. *et al.* Escher: A Web Application for Building, Sharing, and Embedding Data-Rich Visualizations of Biological Pathways. *PLoS Comput Biol* **11**, e1004321 (2015).

93. Bordbar, A., Monk, J. M., King, Z. A. & Palsson, B. O. Constraint-based models predict metabolic and associated cellular functions. *Nat Rev Genet* **15**, 107–120 (2014).

94. Jamialahmadi, O., Hashemi-Najafabadi, S., Motamedian, E., Romeo, S. & Bagheri, F. A benchmark-driven approach to reconstruct metabolic networks for studying cancer metabolism. *PLoS Comput Biol* **15**, e1006936 (2019).

95. Gu, C., Kim, G. B., Kim, W. J., Kim, H. U. & Lee, S. Y. Current status and applications of genome-scale metabolic models. *Genome Biol* **20**, 121 (2019).

96. Opdam, S. *et al.* A Systematic Evaluation of Methods for Tailoring Genome-Scale Metabolic Models. *Cell Syst* **4**, 318-329.e6 (2017).

97. Kim, B., Kim, W. J., Kim, D. I. & Lee, S. Y. Applications of genome-scale metabolic network model in metabolic engineering. *J Ind Microbiol Biotechnol* **42**, 339–348 (2015).

98. Pacheco, M. P. *et al.* Identifying and targeting cancer-specific metabolism with network-based drug target prediction. *EBioMedicine* **43**, 98–106 (2019).

99. Bintener, T. *et al.* Metabolic modelling-based in silico drug target prediction identifies six novel repurposable drugs for melanoma. *Cell Death Dis* **14**, 468 (2023).

100. Bintener, T., Pacheco, M. P., Kishk, A., Didier, J. & Sauter, T. Drug Target Prediction Using Context-Specific Metabolic Models Reconstructed from rFASTCORMICS. in 221–240 (2022). doi:10.1007/978-1-0716-2513-2_17.

101. Becker, S. A. & Palsson, B. O. Context-Specific Metabolic Networks Are Consistent with Experiments. *PLoS Comput Biol* **4**, e1000082 (2008).

102. Zur, H., Ruppin, E. & Shlomi, T. iMAT: an integrative metabolic analysis tool. *Bioinformatics* **26**, 3140–3142 (2010).

103. Casini, I. *et al.* An integrated systems biology approach reveals differences in formate metabolism in the genus Methanothermobacter. *iScience* **26**, 108016 (2023).

104. Schäffer, D. E. *et al.* Microbial gene expression analysis of healthy and cancerous esophagus uncovers bacterial biomarkers of clinical outcomes. *ISME Communications* **3**, (2023).

105. Blazier, A. S. & Papin, J. A. Integration of expression data in genome-scale metabolic network reconstructions. *Front Physiol* **3**, (2012).

106. Heirendt, L. *et al.* Creation and analysis of biochemical constraint-based models using the COBRA Toolbox v.3.0. *Nat Protoc* **14**, 639–702 (2019).

107. Ng, R. H. *et al.* Constraint-Based Reconstruction and Analyses of Metabolic Models: Open-Source Python Tools and Applications to Cancer. *Front Oncol* **12**, (2022).

108. Becker, S. A. *et al.* Quantitative prediction of cellular metabolism with constraint-based models: the COBRA Toolbox. *Nat Protoc* **2**, 727–738 (2007).

109. Lewis, N. E., Nagarajan, H. & Palsson, B. O. Constraining the metabolic genotype–phenotype relationship using a phylogeny of in silico methods. *Nat Rev Microbiol* **10**, 291–305 (2012).

110. Orth, J. D., Thiele, I. & Palsson, B. Ø. What is flux balance analysis? *Nat Biotechnol* **28**, 245–248 (2010).

111. Mahadevan, R. & Schilling, C. H. The effects of alternate optimal solutions in constraint-based genome-scale metabolic models. *Metab Eng* **5**, 264–276 (2003).

112. Gudmundsson, S. & Thiele, I. Computationally efficient flux variability analysis. *BMC Bioinformatics* **11**, 489 (2010).

113. Lewis, N. E. *et al.* Omic data from evolved *E. coli* are consistent with computed optimal growth from genome-scale models. *Mol Syst Biol* **6**, (2010).

114. Megchelenbrink, W., Huynen, M. & Marchiori, E. optGpSampler: An Improved Tool for Uniformly Sampling the Solution-Space of Genome-Scale Metabolic Networks. *PLoS One* **9**, e86587 (2014).

115. Smith, R. L. Efficient Monte Carlo Procedures for Generating Points Uniformly Distributed over Bounded Regions. *Oper Res* **32**, 1296–1308 (1984).

116. Kaufman, D. E. & Smith, R. L. Direction Choice for Accelerated Convergence in Hit-and-Run Sampling. *Oper Res* **46**, 84–95 (1998).

117. McGarrity, S. *et al.* Metabolic systems analysis of LPS induced endothelial dysfunction applied to sepsis patient stratification. *Sci Rep* **8**, 6811 (2018).

118. Bidkhori, G. *et al.* Metabolic Network-Based Identification and Prioritization of Anticancer Targets Based on Expression Data in Hepatocellular Carcinoma. *Front Physiol* **9**, (2018).

119. Agren, R. *et al.* Identification of anticancer drugs for hepatocellular carcinoma through personalized genome-scale metabolic modeling. *Mol Syst Biol* **10**, (2014).

120. Tanguy Margaux & Duflot, T. Approches multi-omiques pour la détermination de nouvelles cibles thérapeutiques dans le rétrécissement aortique calcifié. (Université De Rouen Normandie, Normandie, 2021).

121. Zielinski, D. C. *et al.* Systems biology analysis of drivers underlying hallmarks of cancer cell metabolism. *Sci Rep* **7**, 41241 (2017).

122. Pedregosa, F. Scikit-learn: Machine learning in Python. *Journal of machine learning research* **12**, 2925–2930 (2011).

123. The MathWorks Inc. MATLAB (R2022b). *The MathWorks Inc* (2022).

124. Thiele, I. *et al.* A community-driven global reconstruction of human metabolism. *Nat Biotechnol* **31**, 419–425 (2013).

125. Megchelenbrink, W., Huynen, M. & Marchiori, E. optGpSampler: An Improved Tool for Uniformly Sampling the Solution-Space of Genome-Scale Metabolic Networks. *PLoS One* **9**, e86587 (2014).

126. Addabbo, F. *et al.* Glutamine Supplementation Alleviates Vasculopathy and Corrects Metabolic Profile in an In Vivo Model of Endothelial Cell Dysfunction. *PLoS One* **8**, e65458 (2013).

127. Draoui, N., de Zeeuw, P. & Carmeliet, P. Angiogenesis revisited from a metabolic perspective: role and therapeutic implications of endothelial cell metabolism. *Open Biol* **7**, 170219 (2017).

128. Plaitakis, A., Kalef-Ezra, E., Kotzamani, D., Zaganas, I. & Spanaki, C. The Glutamate Dehydrogenase Pathway and Its Roles in Cell and Tissue Biology in Health and Disease. *Biology (Basel)* **6**, 11 (2017).

129. Pircher, A., Treps, L., Bodrug, N. & Carmeliet, P. Endothelial cell metabolism: A novel player in atherosclerosis? Basic principles and therapeutic opportunities. *Atherosclerosis* **253**, 247–257 (2016).

130. Csuka, P. *et al.* Immobilization of the Aspartate Ammonia-Lyase from *Pseudomonas fluorescens* R124 on Magnetic Nanoparticles: Characterization and Kinetics. *ChemBioChem* **23**, (2022).

131. Castegna, A. & Menga, A. Glutamine Synthetase: Localization Dictates Outcome. *Genes (Basel)* **9**, 108 (2018).

132. Dimou, A., Tsimihodimos, V. & Bairaktari, E. The Critical Role of the Branched Chain Amino Acids (BCAAs) Catabolism-Regulating Enzymes, Branched-Chain Aminotransferase (BCAT) and Branched-Chain α-Keto Acid Dehydrogenase (BCKD), in Human Pathophysiology. *Int J Mol Sci* **23**, 4022 (2022).

133. Li, M., Wu, Y. & Ye, L. The Role of Amino Acids in Endothelial Biology and Function. *Cells* **11**, 1372 (2022).

134. Holeček, M. Branched-chain amino acids in health and disease: metabolism, alterations in blood plasma, and as supplements. *Nutr Metab (Lond)* **15**, 33 (2018).

135. Yu, D. *et al.* The adverse metabolic effects of branched-chain amino acids are mediated by isoleucine and valine. *Cell Metab* **33**, 905-922.e6 (2021).

136. Yamaguchi, A., Botta, E. & Holinstat, M. Eicosanoids in inflammation in the blood and the vessel. *Front Pharmacol* **13**, (2022).

137. Bozza, P. T., Bakker-Abreu, I., Navarro-Xavier, R. A. & Bandeira-Melo, C. Lipid body function in eicosanoid synthesis: An update. *Prostaglandins, Leukotrienes and Essential Fatty Acids (PLEFA)* **85**, 205–213 (2011).

138. Kong, D. & Yu, Y. Prostaglandin D2 signaling and cardiovascular homeostasis. *J Mol Cell Cardiol* **167**, 97–105 (2022).

139. Hanna, V. S. & Hafez, E. A. A. Synopsis of arachidonic acid metabolism: A review. *J Adv Res* **11**, 23–32 (2018).

140. Wang, B. *et al.* Metabolism pathways of arachidonic acids: mechanisms and potential therapeutic targets. *Signal Transduct Target Ther* **6**, 94 (2021).

141. Zheng, Z. *et al.* The biological role of arachidonic acid 12-lipoxygenase (ALOX12) in various human diseases. *Biomedicine & Pharmacotherapy* **129**, 110354 (2020).

142. Lee, H. S. *et al.* Prostaglandin D2 stimulates phenotypic changes in vascular smooth muscle cells. *Exp Mol Med* **51**, 1–10 (2019).

143. Fan, Y. *et al.* Comprehensive Metabolomic Characterization of Coronary Artery Diseases. *J Am Coll Cardiol* **68**, 1281–1293 (2016).

144. van Driel, B. O. van *et al.* Metabolomics in Severe Aortic Stenosis Reveals Intermediates of Nitric Oxide Synthesis as Most Distinctive Markers. *Int J Mol Sci* **22**, 3569 (2021).

145. Surendran, A. *et al.* Metabolomic Signature of Human Aortic Valve Stenosis. *JACC Basic Transl Sci* **5**, 1163–1177 (2020).

146. Martínez-Reyes, I. & Chandel, N. S. Mitochondrial TCA cycle metabolites control physiology and disease. *Nat Commun* **11**, 102 (2020).

147. Mashimo, T. *et al.* Acetate Is a Bioenergetic Substrate for Human Glioblastoma and Brain Metastases. *Cell* **159**, 1603–1614 (2014).

148. Schug, Z. T. *et al.* Acetyl-CoA Synthetase 2 Promotes Acetate Utilization and Maintains Cancer Cell Growth under Metabolic Stress. *Cancer Cell* **27**, 57–71 (2015).

149. Ciraku, L. *et al.* O-GlcNAc transferase regulates glioblastoma acetate metabolism via regulation of CDK5-dependent ACSS2 phosphorylation. *Oncogene* **41**, 2122–2136 (2022).

150. Selak, M. A. *et al.* Succinate links TCA cycle dysfunction to oncogenesis by inhibiting HIF-α prolyl hydroxylase. *Cancer Cell* **7**, 77–85 (2005).

151. Altman, B. J., Stine, Z. E. & Dang, C. V. From Krebs to clinic: glutamine metabolism to cancer therapy. *Nat Rev Cancer* **16**, 619–634 (2016).

152. Metallo, C. M. *et al.* Reductive glutamine metabolism by IDH1 mediates lipogenesis under hypoxia. *Nature* **481**, 380–384 (2012).

153. Ward, P. S. *et al.* The Common Feature of Leukemia-Associated IDH1 and IDH2 Mutations Is a Neomorphic Enzyme Activity Converting α-Ketoglutarate to 2-Hydroxyglutarate. *Cancer Cell* **17**, 225–234 (2010).

154. Fong, G.-H. & Takeda, K. Role and regulation of prolyl hydroxylase domain proteins. *Cell Death Differ* **15**, 635–641 (2008).

155. Yang, W.-H., Qiu, Y., Stamatatos, O., Janowitz, T. & Lukey, M. J. Enhancing the Efficacy of Glutamine Metabolism Inhibitors in Cancer Therapy. *Trends Cancer* **7**, 790–804 (2021).

156. Kim, M. K. & Lun, D. S. Methods for integration of transcriptomic data in genome-scale metabolic models. *Comput Struct Biotechnol J* **11**, 59–65 (2014).

157. Pacheco, M. P., Ji, J., Prohaska, T., García, M. M. & Sauter, T. scFASTCORMICS: A Contextualization Algorithm to Reconstruct Metabolic Multi-Cell Population Models from Single-Cell RNAseq Data. *Metabolites* **12**, 1211 (2022).